# Optical Mining – A Spallation Mining Model

By: Timofey Broslav[1], Chris Dreyer[1], Joel Sercel[2]

[1]Colorado School of Mines, 1500 Illinois St, Golden, CO 80401

[2]TransAstranautica Corporation, 13539 Desmond St., Los Angeles, CA 91331

# Optical Mining and Thermal Spalling

*The Optical Mining Process*

- The Optical Mining process was developed by Trans-Astra (Trans Astronautica Corporation) as a non-contact method to mine carbonaceous chondritic asteroids for water and other volatiles with collected and focused solar light [1]

- Utilizes the thermal spalling phenomenon to break away fragments of an asteroid's surface and concurrently heat them to release volatiles through dehydroxilation, and other, reactions

- Improvement over physical excavation methods (due to issues with micro gravity environments), and bulk heating methods

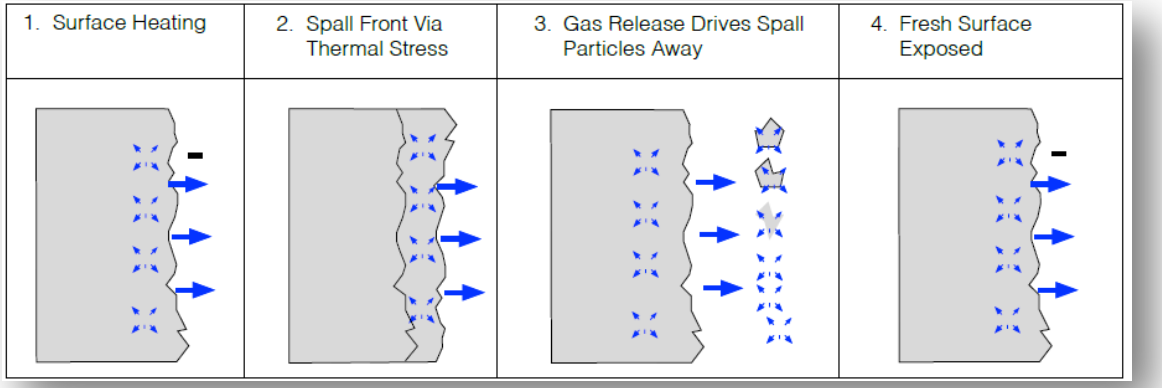


Optically-Induced Thermal Spalling as Conceptualized by Sercel, 2016 [1]

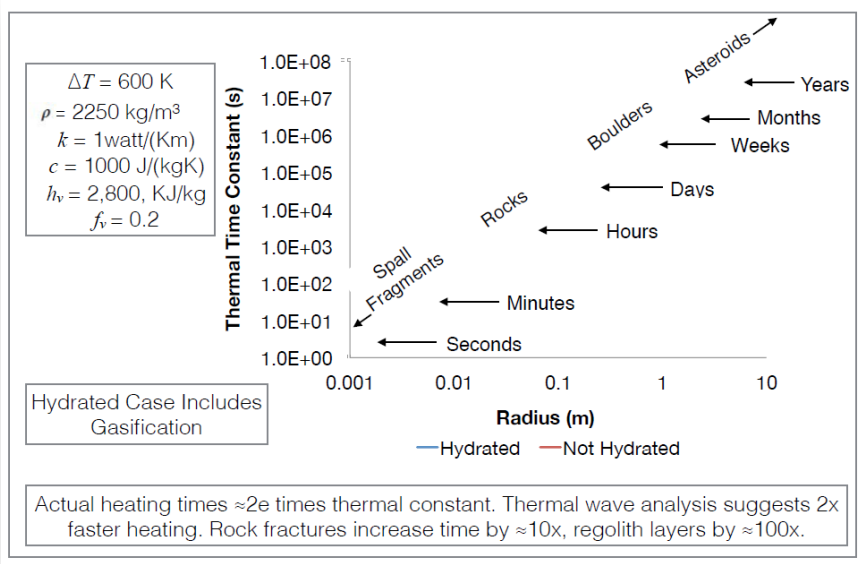


Bulk Heating of Asteroids [1]

# Overview of This Work

*The purpose of my work is to improve the understanding of Optical Mining in excavation and volatile production (e.g water) from chondritic asteroids simulants*

## Spallation Mining Model

- Models the complex Optical Mining process utilizing 1-D heat transfer, thermo-elastic stress, and Weibull statistical failure
- Uses experimental data from testing of the Optical Mining process
- Predicts excavation rates utilizing the Optical Mining process on a given body
- Predicts response modes of a body undergoing Optical Mining ( e.g melting, bulk heating)
- Investigates effect of irradiance distributions on excavation rates during the mining process

# Thermal Spalling and Optical Mining

*Thermal Spalling*

- Thermal spalling is the process of material failure from thermal stresses ((1) adjacent material compression from thermal gradients (2) and thermal expansion mismatch ) that ejects small fragments of material from a larger body [2-3]

$$(1)\ \sigma_{Thermal} = \frac{\alpha E \Delta T}{1-\nu} \qquad (2)\ \sigma_{T.E\ mismatch} = E\Delta\beta\Delta T$$

- Explosive spalling due to vapor buildup is possible in some materials
- Buckling failure theory is widely agreed upon description of thermal spalling failure process [3 –7]
- There are a variety of thermomechanical and statistical variables that are involved in thermal spalling [3,7-12]

Optical Mining of an Asteroid Simulant Cake (Nectar A) via Thermal Spalling

# Optical Mining and Thermal Spalling

*Buckling Mechanism and Weibull Statistical Failure*

- As thermal wave penetrates material, more volume becomes stressed. These stresses coalesce in pre-existing flaws to form fractures that spread out and cause material to buckle [2]
- Weibull statistical failure can be used to predict probability of reaching a flaw in a volume of a stressed material and lead to failure [3] (size-strength relationship of rocks)

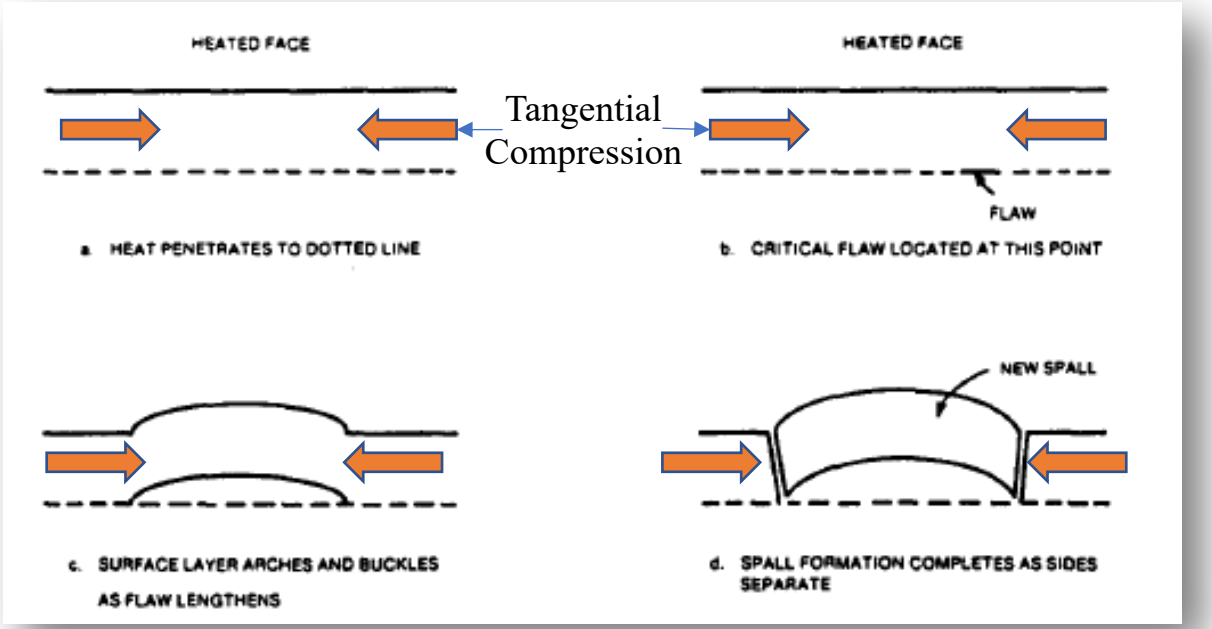


Phases of Buckling Failure [2]

$$Pr(\sigma) = 1 - e^{\left[-\int_0^V (n(\sigma))^m dV\right]}$$
$$n(\sigma) = \left(\frac{\sigma}{\sigma_o}\right)^m$$

(Pr) – Probability of Failure (failure at Pr ≥ 0.5)
(V) – Volume of stressed material, ($m^3$)
(σ) – Applied Compressive Stress, (Pa)
(n) – number of weak points per unit volume which can cause failure at a stress σ, ($m^{-3}$)
($\sigma_o$) – Inherent compressive strength of 1 unit dimensions in volume (Pa)
($m$) – Homogeneity of sample (higher = more homogenous)

# The Optical Mining Testbed

*Testing Methods*

Nectar "A" Simulant Cake

- Two subtypes (Nectar A/B due to differences in sources of minerals)
- CI/CM Asteroid composition
- Bulk Density: 1.1 – 1.3 g/cm$^3$
- Diameter: 12"

"Apollo" Vacuum Chamber

- Quartz window for light propagation
- Volume: 1 m$^3$
- Test Pressure Range: 60 mtorr -3 torr

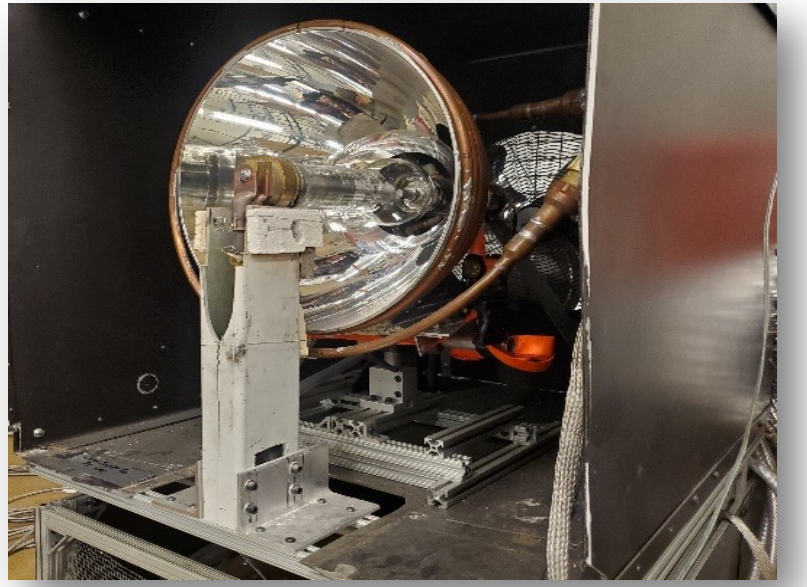

15 kW Xenon Arc Lamp and Reflector Assembly within a Protective Shroud

- Incident Flux - 100 W/cm$^2$ to 900 W/cm$^2$
  - ~3 kW total beam power
- Beam Size – 3 cm to 4 cm
- Radial Flux distribution

# The Optical Mining Testbed

*Dimensionless Area vs Dimensionless Irradiance*

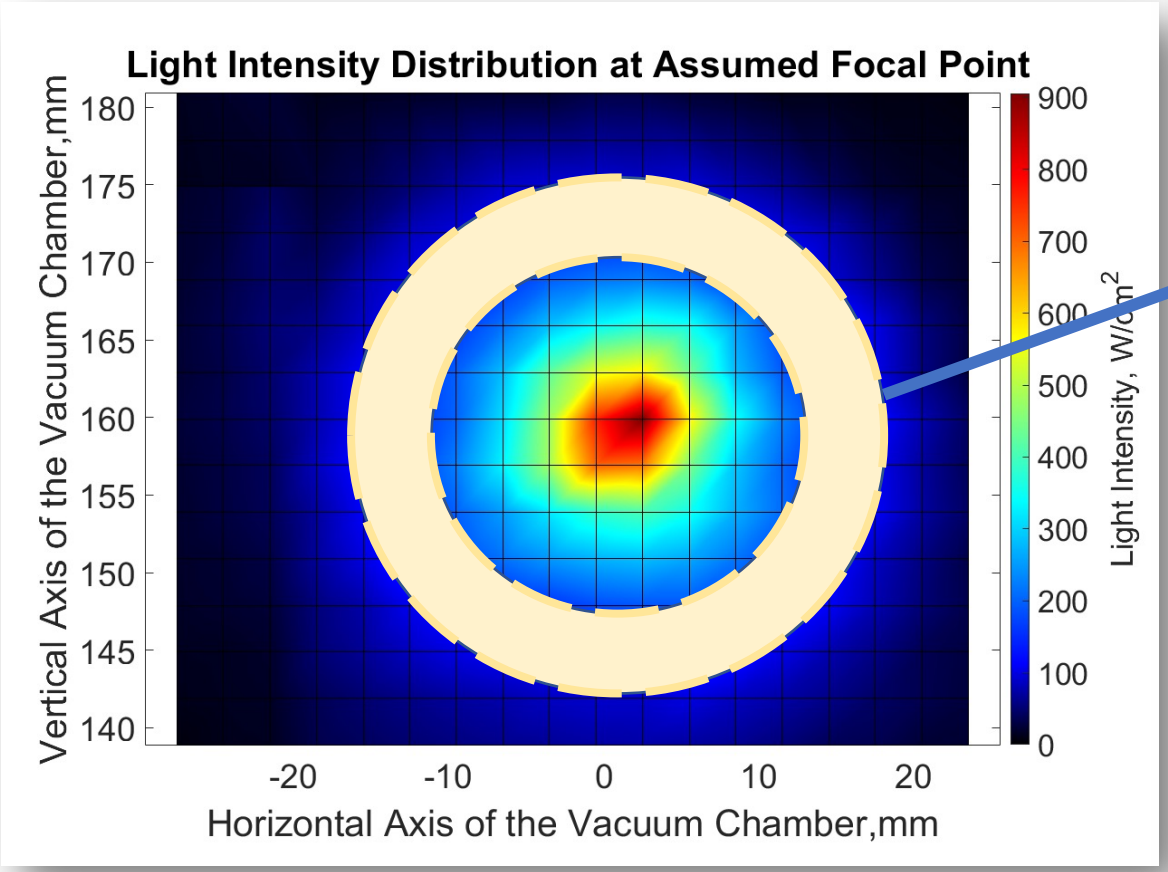


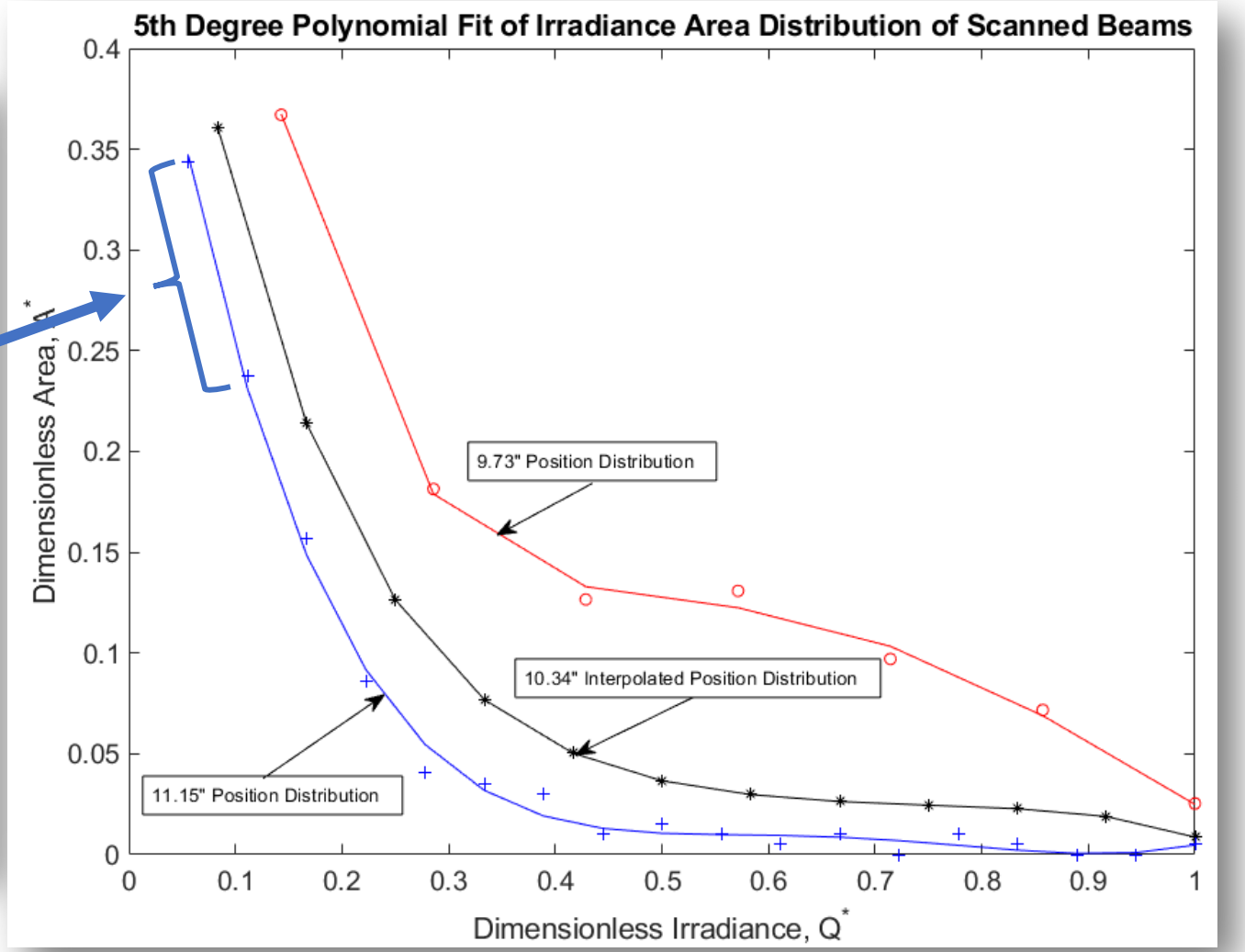

# The Optical Mining Testbed

*Nectar A and Nectar B Responses to Optical Mining*

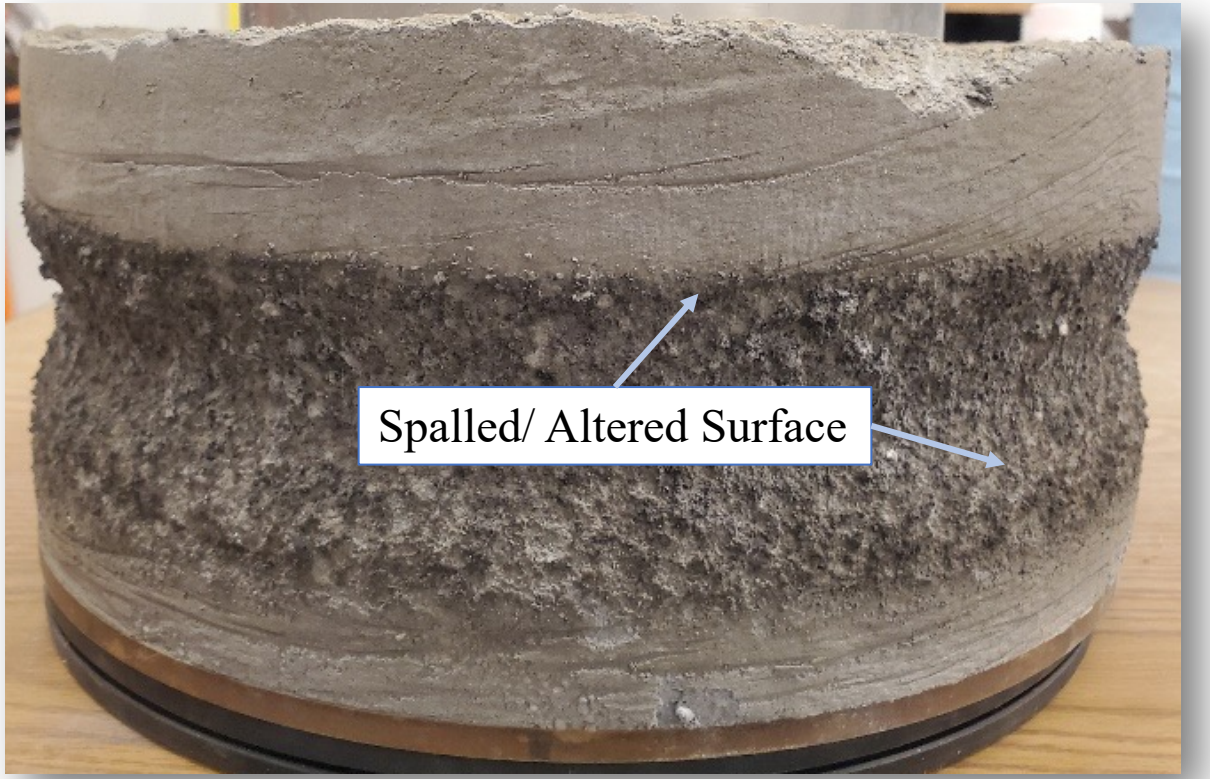


Nectar A Simulant "Cake" Post Test
353.4 W/cm$^2$ Avg. Irr. at FWHM size

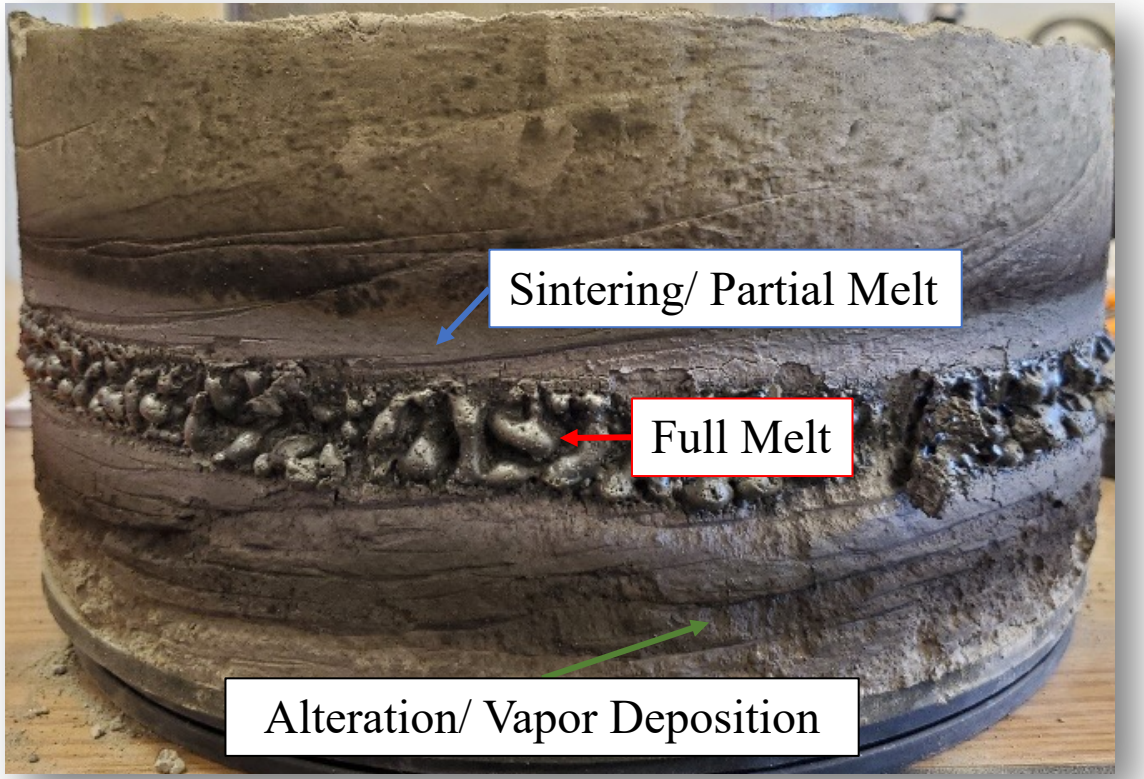


Nectar B Simulant "Cake" Post Test
353.4 W/cm$^2$ Avg. Irr. at FWHM size

It was theorized that the addition of exfoliated Vermiculite to Nectar B led Nectar B to melt at the same irradiance

# The Optical Mining Testbed

*Experimental Excavation Rate Results vs Average Beam Irradiance at Full-Width Half Max (FWHM)*

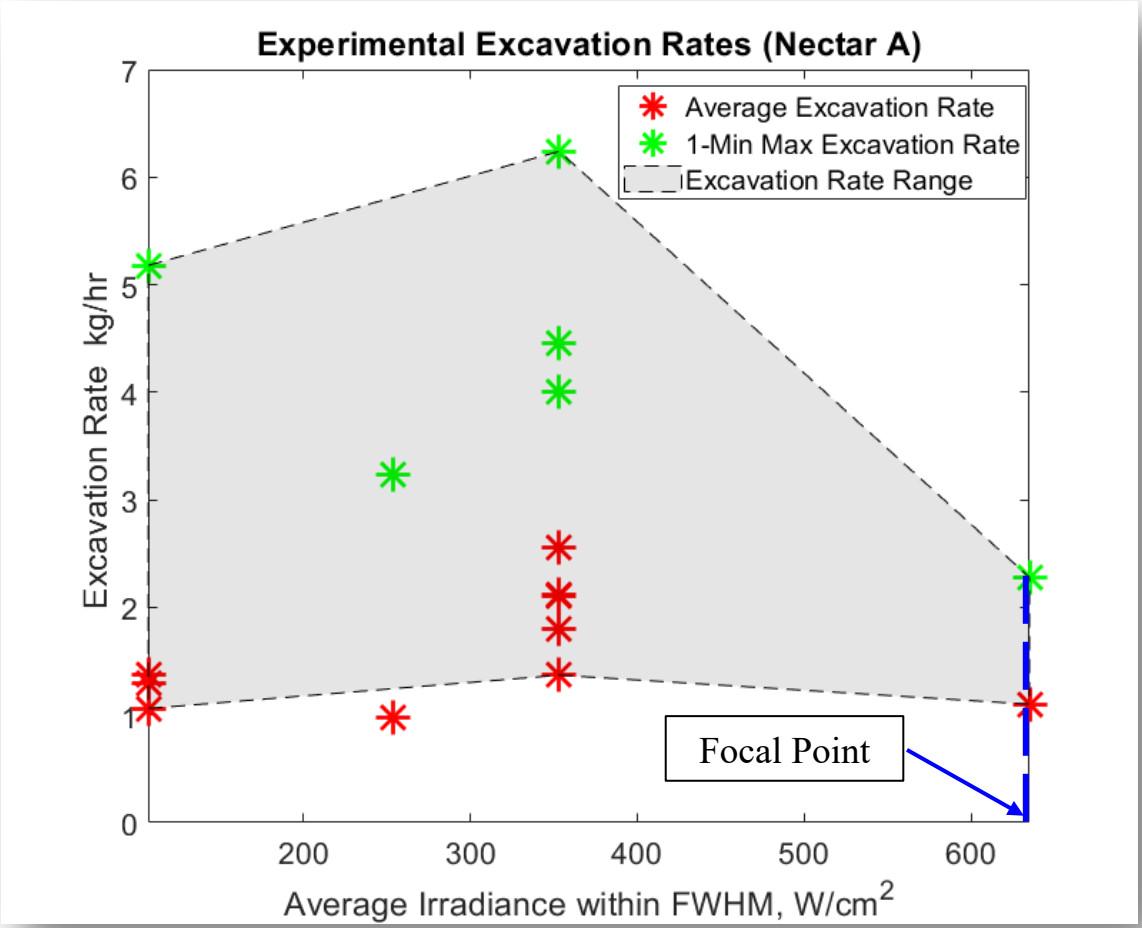


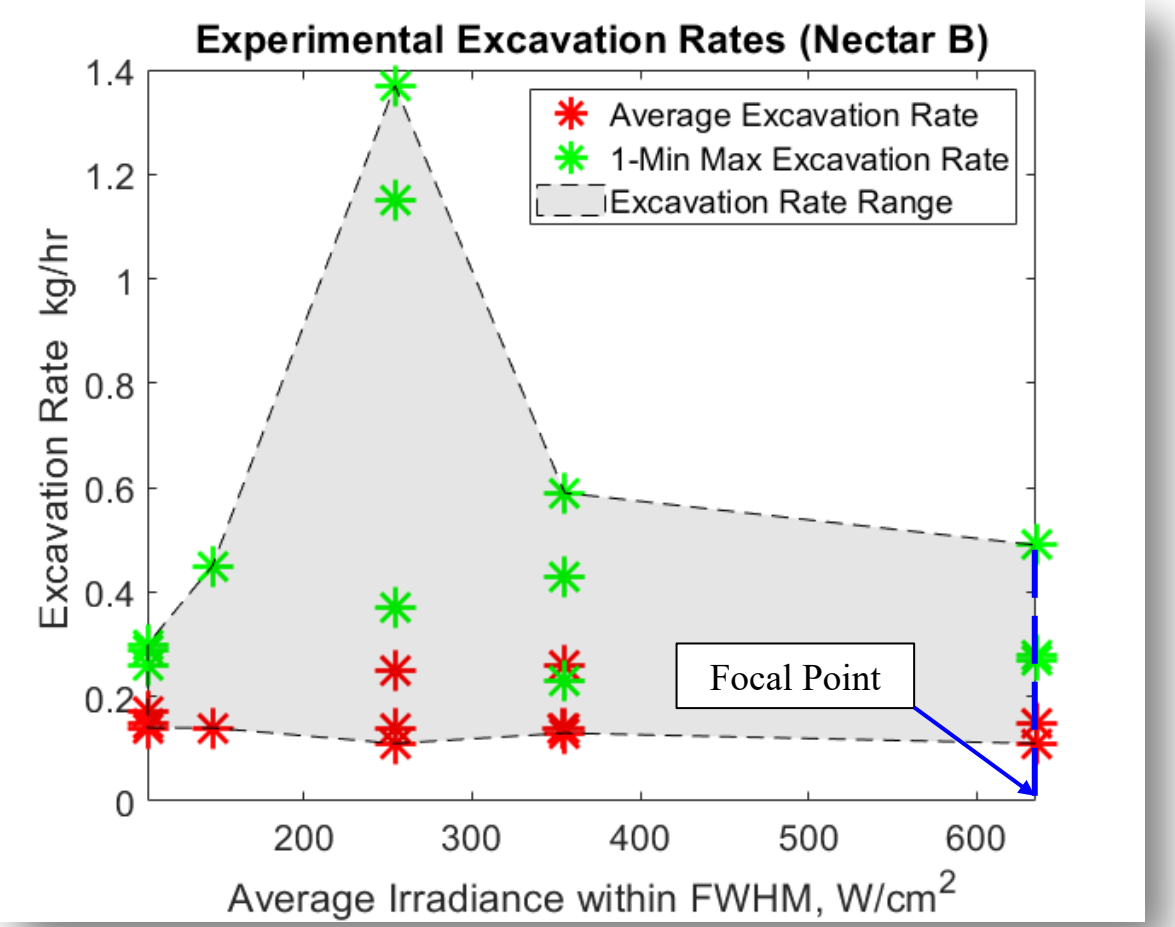


*Averaged and 1-min max excavation rates vs Average Beam Irradiance at Full Width Half Max (FWHM)*

# The Optical Mining Testbed

*Spalled Surface Analysis*

- Microscope analysis of a Nectar A simulant spalled with a FWHM irradiance of 353.4 W/cm$^2$ shows areas of the surface sinter/melt even though it does not appear so with the naked eye
- Modeling of Nectar A excavation should be able to predict this
- May explain the drop off in excavation rate for Nectar A if a higher irradiance would create more areas of sinter/melt zones

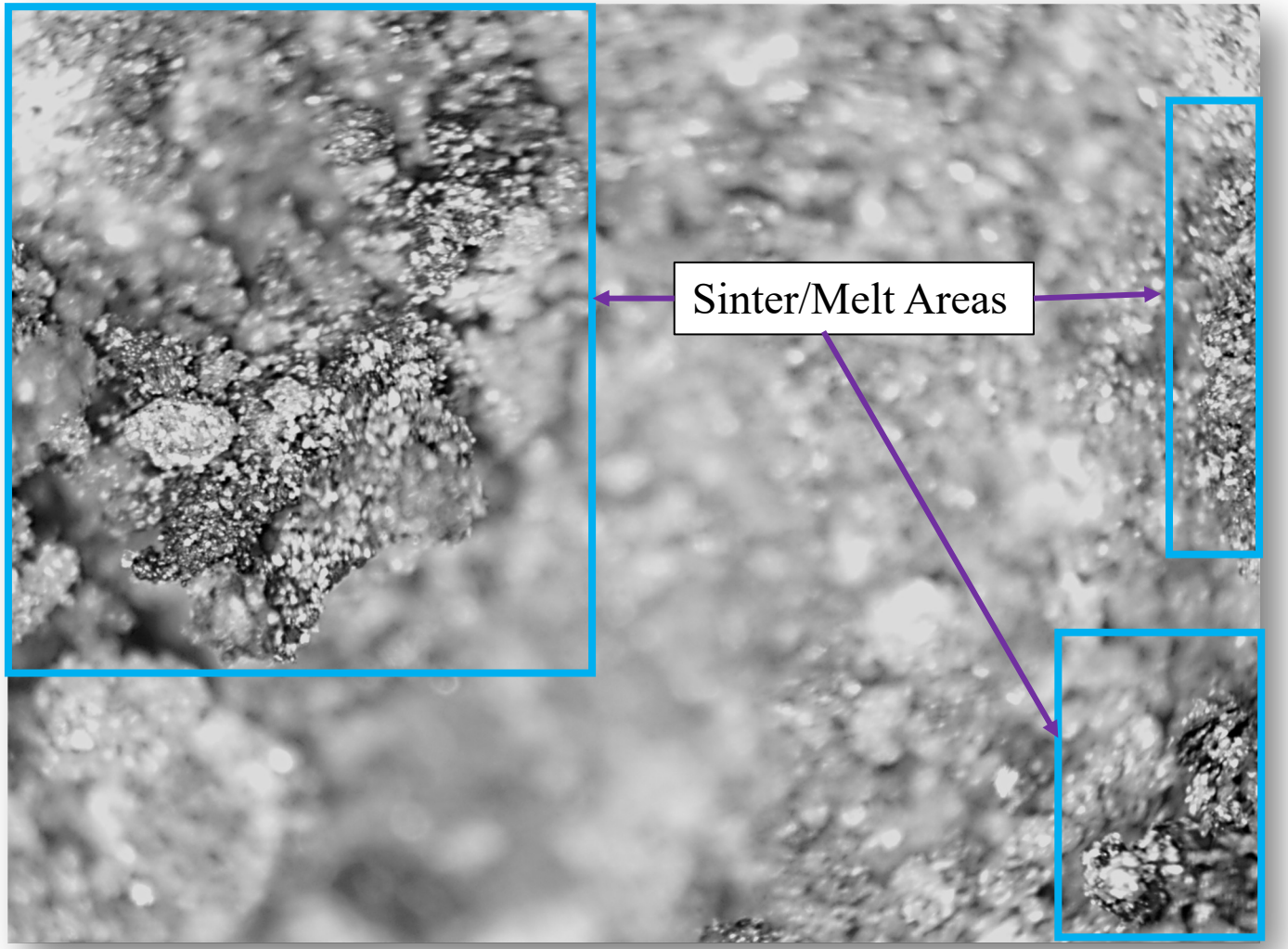


Nectar A Spalled Surface w/ Melt/Sintering 353.4 W/cm$^2$ Avg. Irr. at FWHM size

# Spallation Mining Model

*Overview*

- Heat transfer is modeled using a 1-D forward volume difference method in MATLAB
  - Incorporates irradiance distribution of the impingent beam (split into fractions of the total beam area) as the heat input on surface nodes
- Compressive thermal stresses are computed at each volumetric node transversal to the heat propagation plane assuming plane stress (1)

$$(1)\ \sigma_{Thermal} = \frac{\alpha E \Delta T}{1 - \nu}$$

- Weibull fracture probability is used to predict onset of spallation or fracture from thermal stresses
- Temperature dependent thermal properties based sandstone response temperature change [13]
- Stress relief via surface undulations, brittle-ductile transition, and melting
- Incorporates melt reactions, equilibrium based dehydroxilation and dehydration reactions
- Incorporates morphological effects (Vermiculite Expansion) [14-15]
- Stop Condition based on surface melt percentage exceeding 50 % of the beam area (1167 $^{o}$C)

# Spallation Mining Model

*Ductility and its Effects*

- Surface overheating has been observed in the past during thermal spalling experiments of Granite [16]
  - Attributed to thermal softening of adjacent material
- Ductile-Brittle Transition (Thermal Softening) has been observed to occur for sandstone at around 600 °C [17]
  - Youngs Modulus decrease due to pore collapse
  - Crystal plasticity between minerals adds a higher energy requirement for breaking of bonds and fracture propagation [18-20]
- Reaching this transition temperature would result in a drop in overall stress and an overheating effect as more stress buildup is required due to higher energy requirements of fracture propagation
- The addition of temperature dependent Youngs modulus, and a monotonically decreasing stress modification function, incorporates these effects into the model
  - Stress modification function decreases from 1 to 0 depending on the ductile – melt temperature range chosen (600 - 1177 °C)

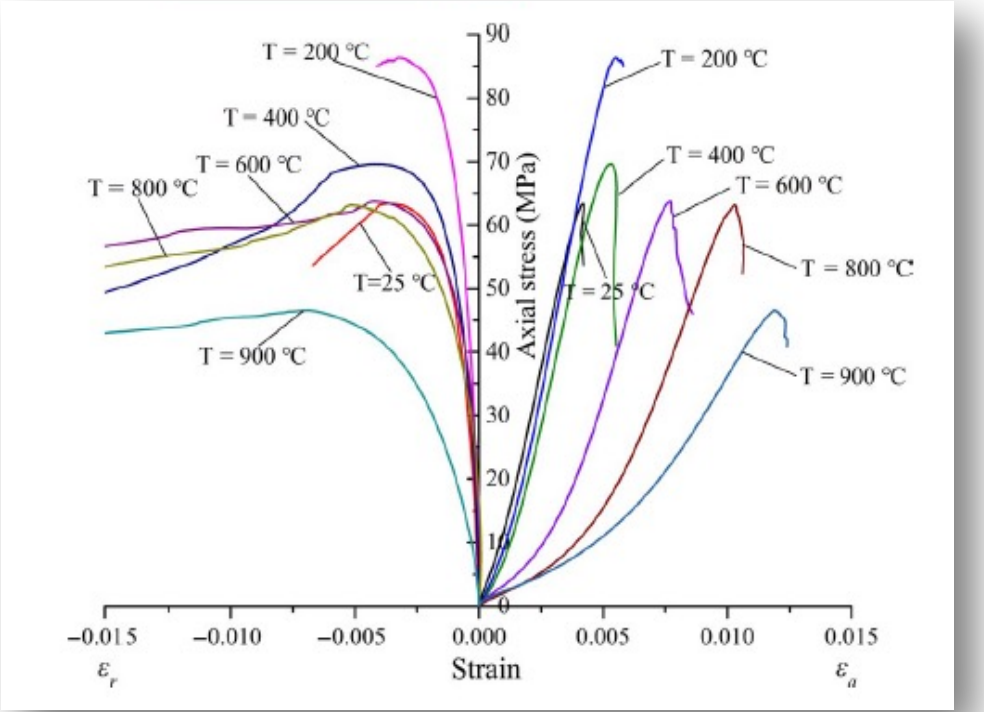


Stress-Strain Curve of Sandstone After Heat Treatment [17]

# Spallation Mining Model

*Beam Irradiance Input*

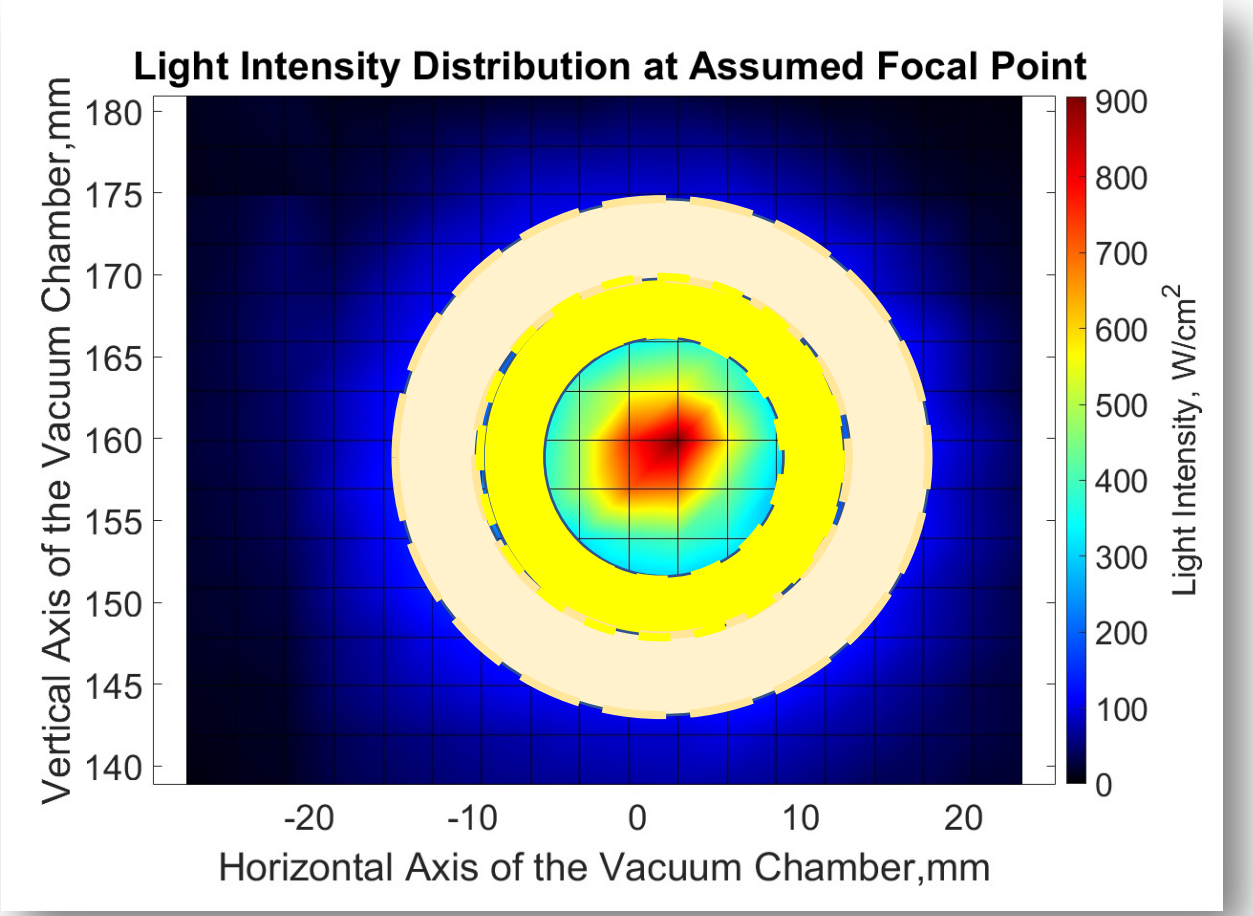


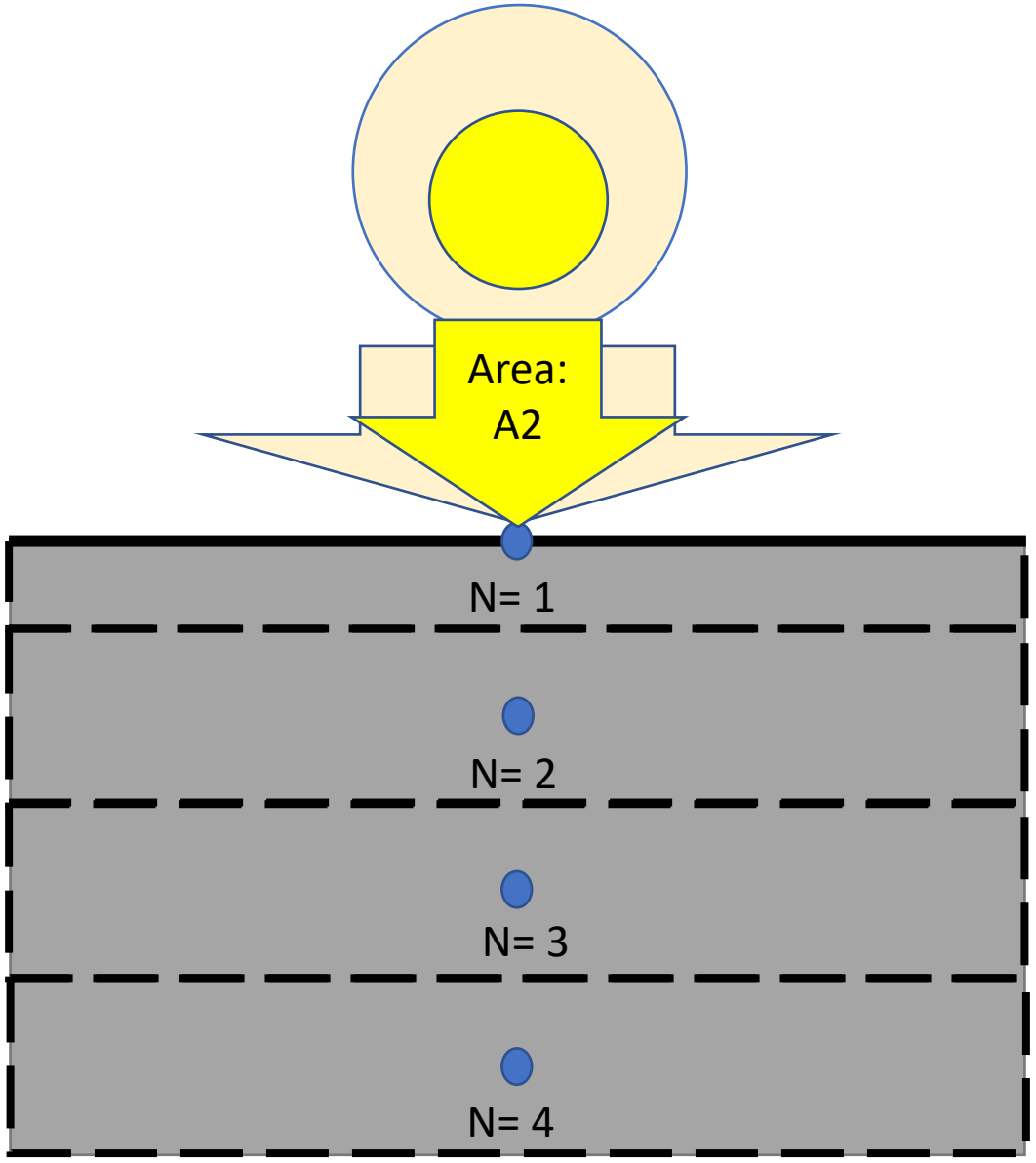


Mesh Diagram of Body

# Spallation Mining Model

*Model Process Flow*

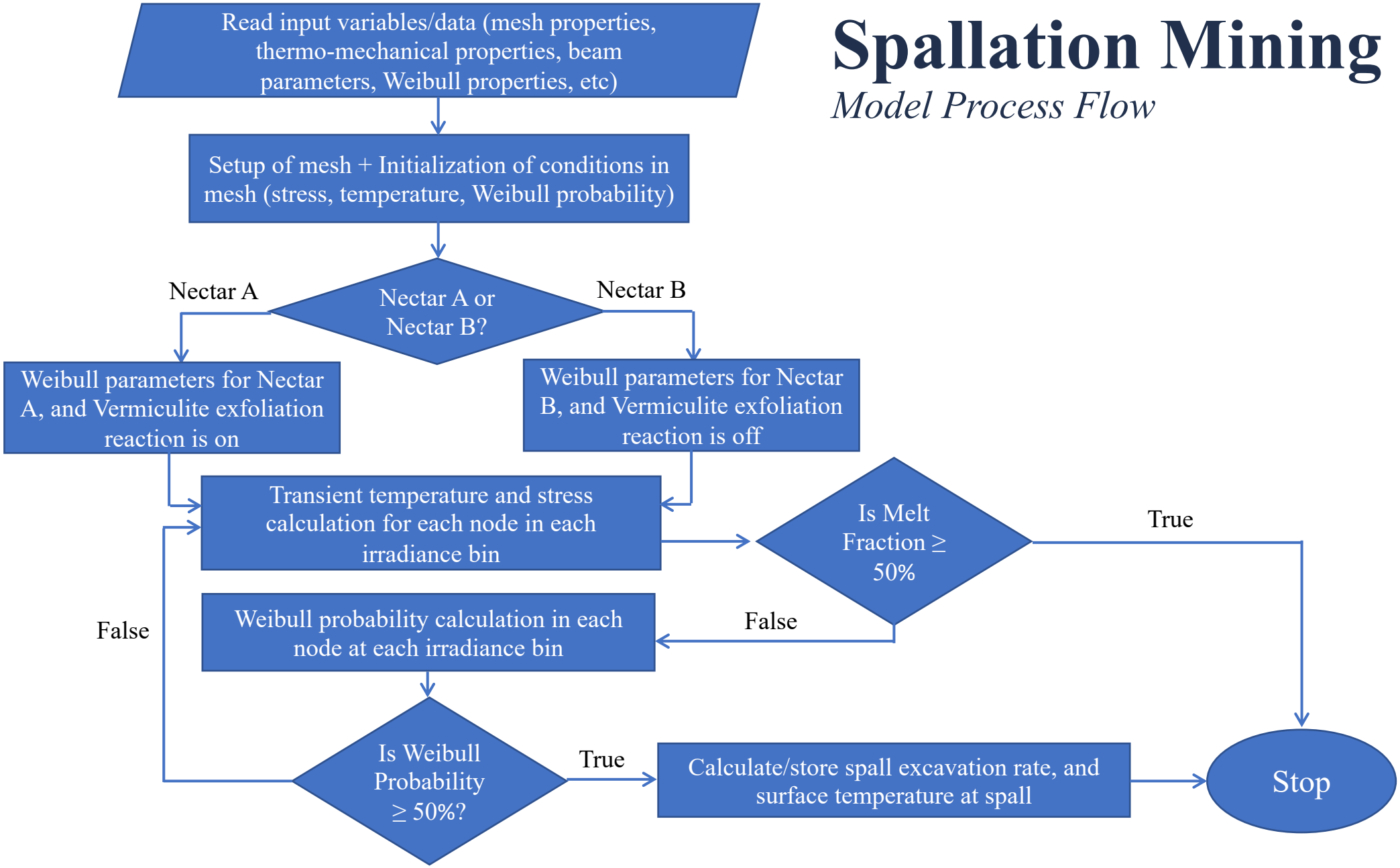

# Spallation Mining Model

*Variation of Input Variables*

- Several mechanical variables of the Nectar simulant were varied to investigate possible parameters that would yield a decrease in excavation at focus
  1. Thermal Expansion
     - ±35 %
  2. Youngs Modulus
     - ±60 %
  3. Heat capacity at room temperature
     - ±12 %
  4. Thermal conductivity in vacuum
     - Drop in thermal conductivity varied from 13% to 56 % drop under vacuum conditions
  5. Percent of stress relief at surface due to roughness
     - 25 - 100 %

# Spallation Mining Model

*Excavation Prediction for Nectar A and Nectar B*

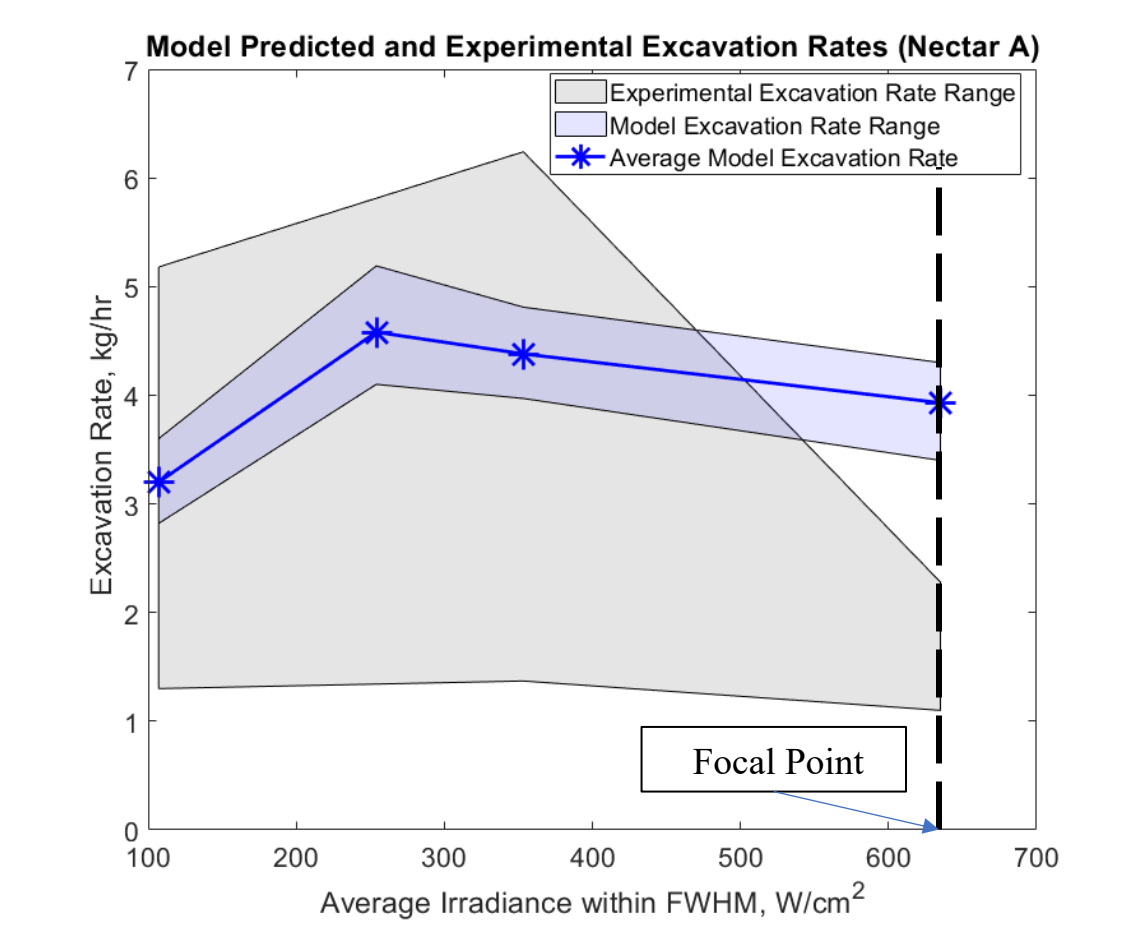


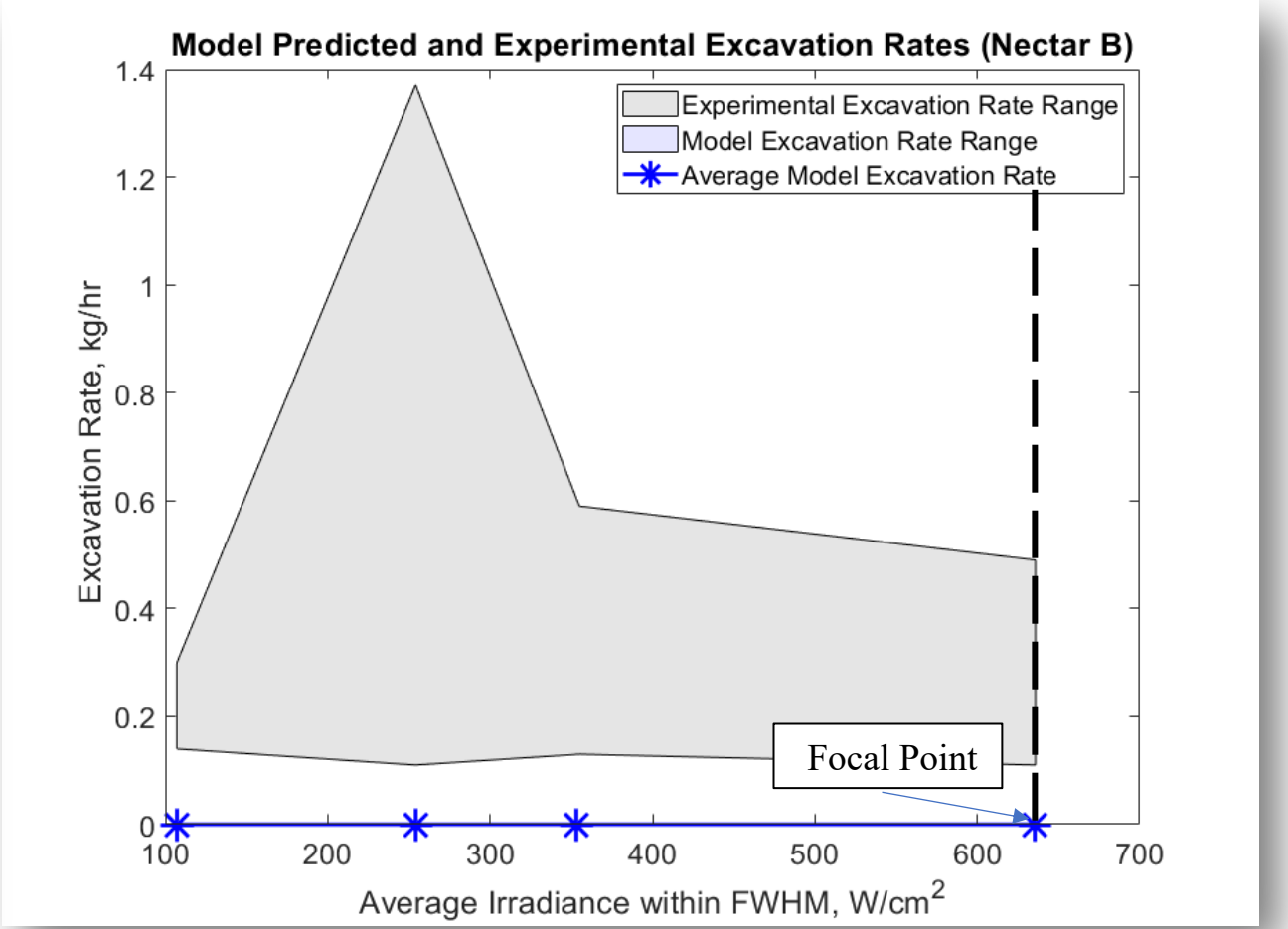

# Spallation Mining Model

*Melt Fraction Prediction*

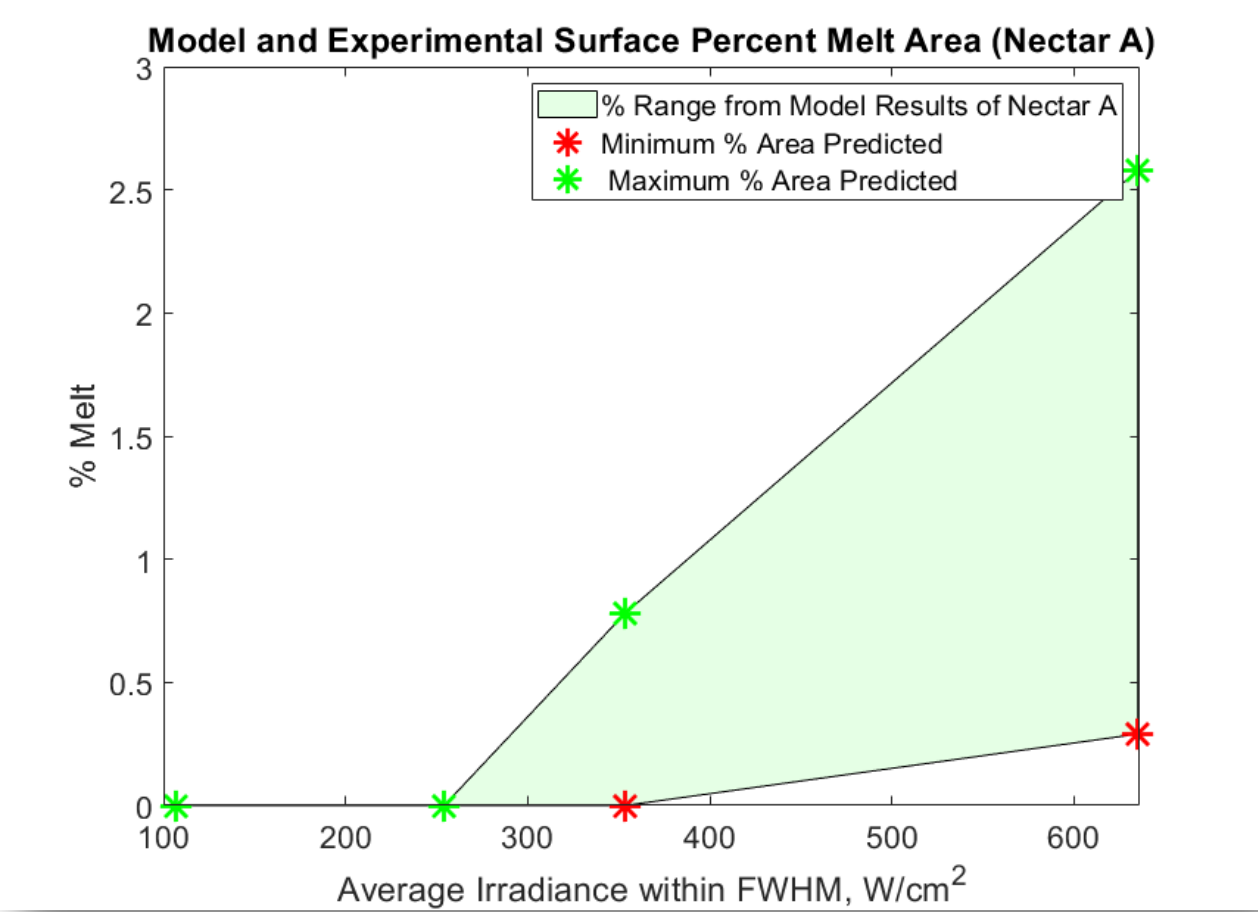


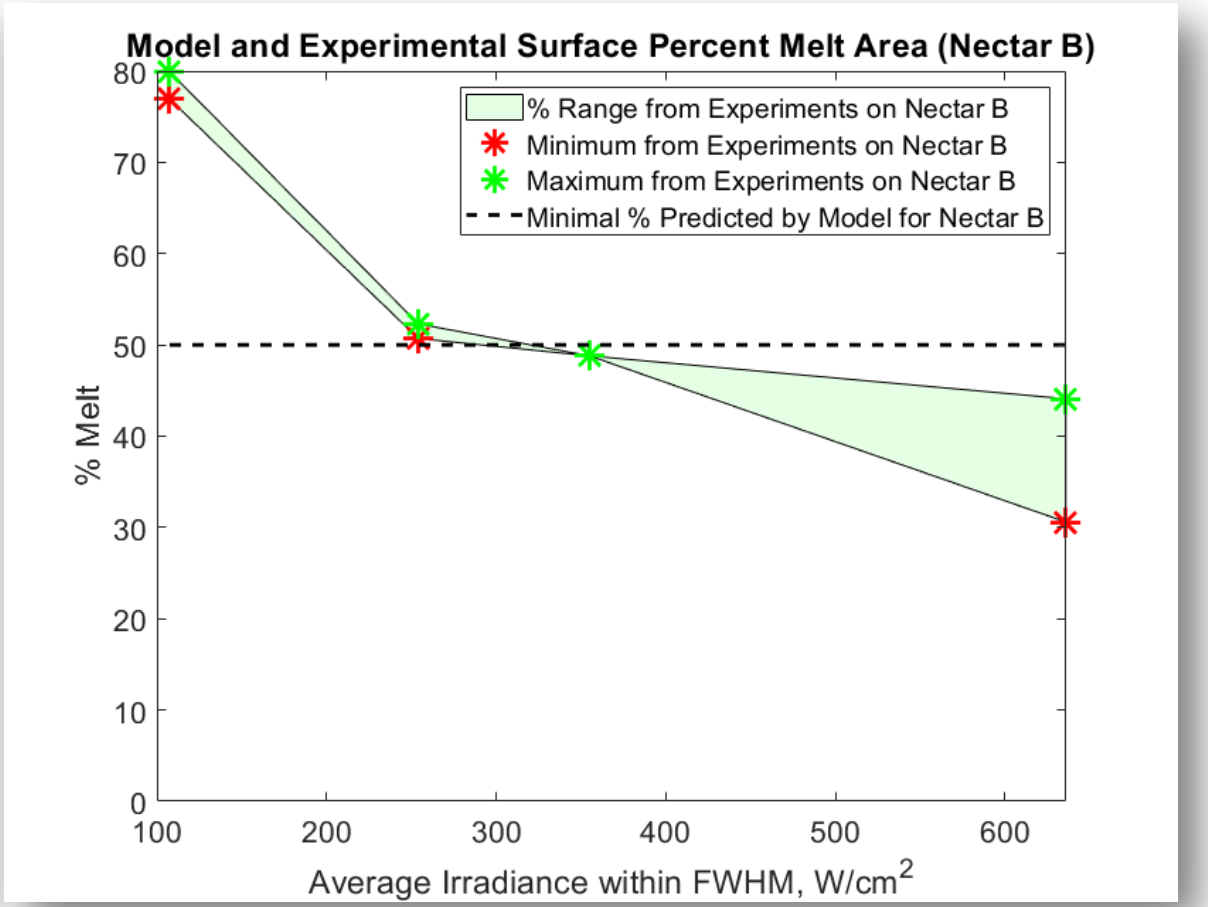

# Conclusions and Lessons Learned

*A Simple Model with Powerful Versatility*

1. The excavation model can 1) predict whether a material will melt or undergo continuous spallation excavation, 2) account for morphological/volatile effects, and 3) predict excavation rate trends given material properties and beam parameters
2. The irradiance distribution within a beam has significant effects on Optical Mining operations
3. Successfully modeling of Optical Mining on asteroid bodies requires semi-accurate property information and knowledge of morphology of asteroid materials present and ductile zone transition boundary
    a) Knowledge of any phase change/reaction that incur a large increase in thermal expansion coefficients(or stress) within a body
4. Measurement of temperature and control of irradiance impingement on the surface is vital to prevent material from reaching ductile/melt temperature transition
5. Organic reactions may form film on optical surfaces, that may hamper mining operations and must be controlled for
    a) Either by removing the film, or preventing its creation

# Questions

*Thank you for listening*

Email: tbroslav@mines.edu

Conceptual Image of Optical Mining (ChatGPT)

# References


1. Sercel, Joel. *APIS: Asteroid Provided In-Situ Supplies*. 2016, www.lpi.usra.edu/sbag/meetings/jun201 6/presentations/sercel.pdf.
2. Preston FW, White HE (1934) Observations on spalling. J Am Ceram Soc 17:137–144
3. Rauenzahn, R.M., and J.W. Tester. “Rock Failure Mechanisms of Flame-Jet Thermal Spallation Drilling—Theory and Experimental Testing.” *International Journal of Rock Mechanics and Mining Sciences & Geomechanics Abstracts*, vol. 26, no. 5, 1989, pp. 381–399., https://doi.org/10.1016/0148-9062(89)90935-2.
4. Dmitriev, A. P., A. D. Sukhanov, and O. N. Tret'yakov. "Calculating the parameters of the thermal drilling process." *Soviet Mining* 5.1 (1969): 26-31.
5. Kolodko, A. Ya. "Thermal stress state and fracture of a mass of rock under nonuniform surface heating." *Soviet Mining* 19.5 (1983): 392-398.
6. Dey, Thomas N., and R. L. Kranz. *Methods for increasing drilling performance of the thermal spallation drilling system*. No. LA-UR-85-831; CONF-850801-11. Los Alamos National Lab., NM (USA), 1985.
7. Lyu, Zehao, et al. "Experimental analysis on characteristics of micro-structure and mineralogy changes in thermal spallation drilling." *Journal of Petroleum Science and Engineering* 167 (2018): 100-109.
8. Goodrich, Hobert R. “Spalling and Loss in Compressive Strength of Fire brick1.” *Journal of the American Ceramic Society*, vol. 10, no. 10, 1927, pp. 784–794., https://doi.org/10.1111/j.1151-2916.1927.tb18470.x.
9. Kingery, W. David. "Factors affecting thermal stress resistance of ceramic materials." *Journal of the American Ceramic Society* 38.1 (1955): 3-15.
10. Mirkovich, V. V. "Experimental study relating thermal conductivity to thermal piercing of rocks." *International Journal of Rock Mechanics and Mining Sciences & Geomechanics Abstracts*. Vol. 5. No. 3. Pergamon, 1968.
11. Nelson, Charles Ray. *Investigation of modes of thermal fracture of some brittle materials*. Diss. Massachusetts Institute of Technology, 1969.
12. Kant, Michael, et al. “A Theory on Thermal Spalling of Rocks with a Focus on Thermal Spallation Drilling.” Journal of Geophysical Research: Solid Earth, 2017, https://doi.org/10.1002/2016jb013800.

# References


13. Robertson, Eugene C. "Thermal properties of rocks." (1988).
14. Sutcu, Mucahit. "Influence of expanded vermiculite on physical properties and thermal conductivity of clay bricks." *Ceramics International* 41.2 (2015): 2819-2827.
15. Petersen, Rasmus R., et al. "Expansion and shrinkage of lightweight vermiculite material at high temperatures." Ceramics International 49.14 (2023): 23605-23611.
16. Wilkinson, M. A., and J. W. Tester. "Experimental measurement of surface temperatures during flame-jet induced thermal spallation." Rock mechanics and rock engineering 26 (1993): 29-62.
17. Lei, Ruide, et al. "The evolution of sandstone microstructure and mechanical properties with thermal damage." Energy Science & Engineering 7.6 (2019): 3058-3075.
18. Wong, Teng-Fong. "Mechanical compaction and the brittle—ductile transition in porous sandstones." Geological Society, London, Special Publications 54.1 (1990): 111-122.
19. Wong, Teng-fong, and Patrick Baud. "The brittle-ductile transition in porous rock: A review." Journal of Structural Geology 44 (2012): 25-53.
20. Cannizzo, Andrea, and Stefano Giordano. "Thermal effects on fracture and the brittle-to-ductile transition." Physical Review E 107.3 (2023): 035001.

# Backup Slides

# The Optical Mining Testbed

*Experiment Layout*

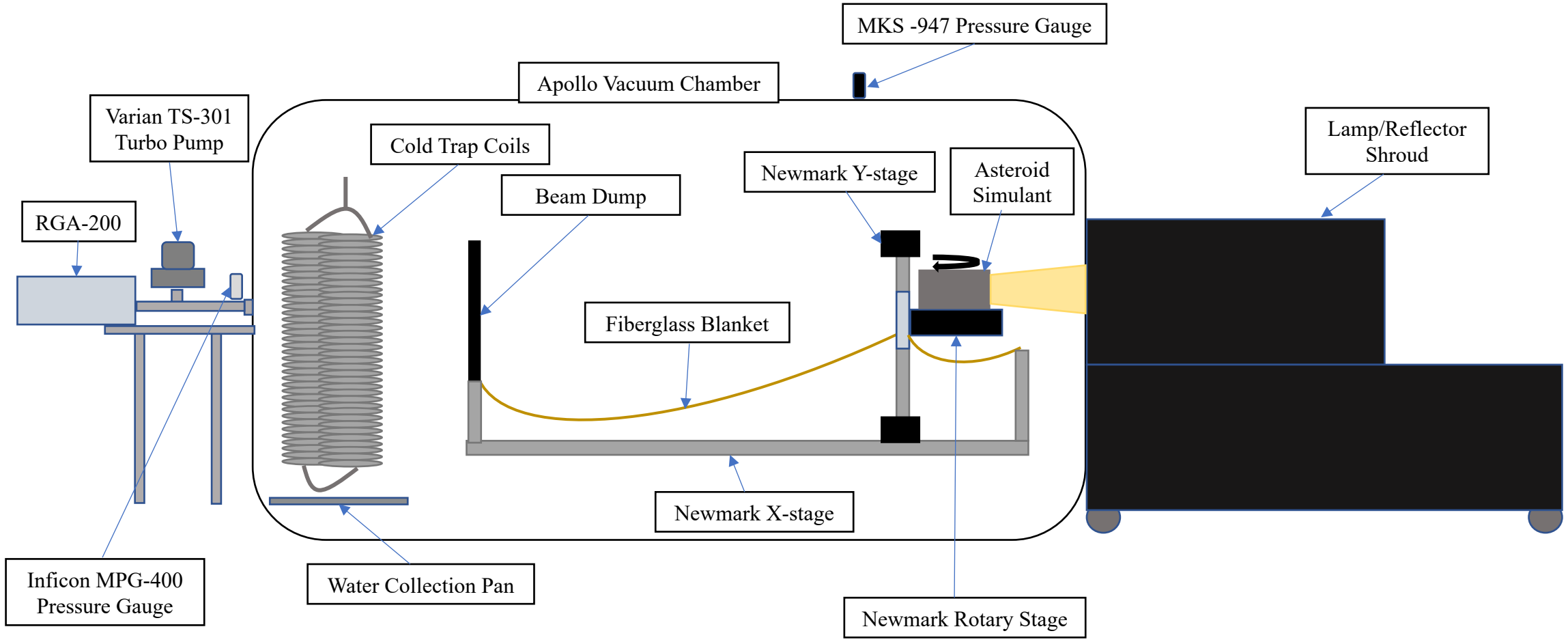

# The Optical Mining Testbed

*Testing Methods*

Experiment Test Bed on a Cart

- Motor Control – X and Y axes
- Rotary Stage
- Fiberglass Blanket for excavated mass capture

Steel Cold Trap Coils for Volatile Capture

- Volatile Capture – $H_2O$, $CO_2$, others
- Pressure Regulator
- Volatile Capture + RGA data = Water Production

# The Optical Mining Testbed

*Weibull Parameter Testing*

Core Press/Mold Used to Manufacture Tested Cores

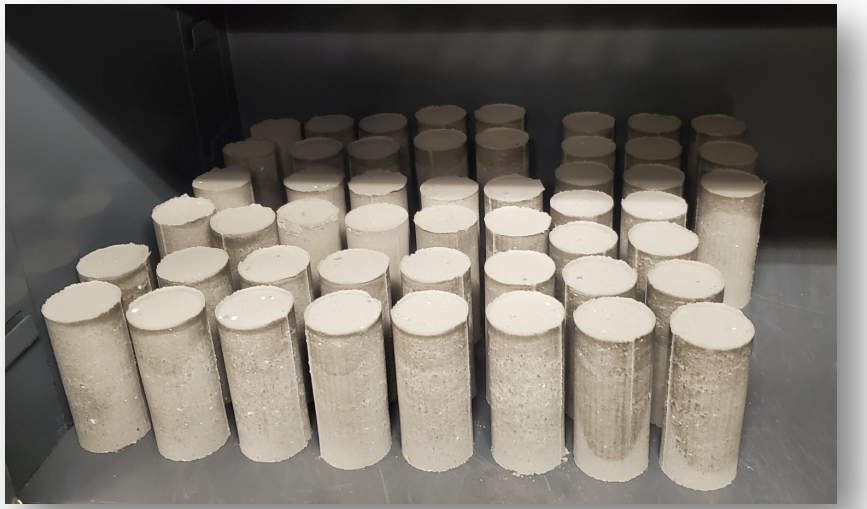

Cores Air Drying

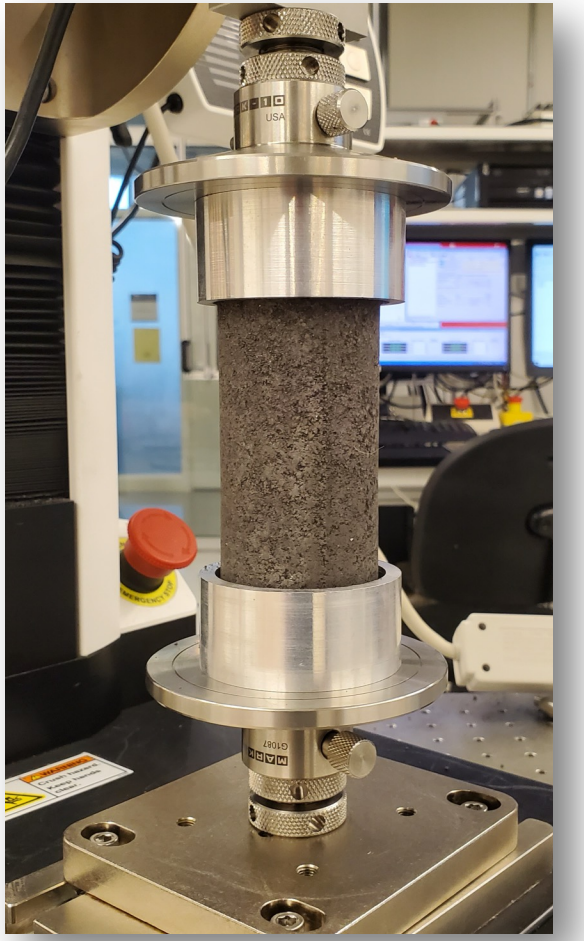

Setup of a Compressive Strength Test (Neoprene Caps Not Shown)

# The Optical Mining Testbed

*Testing Conducted*

- Because of the complexity of running tests, 50 Optical Mining tests have been conducted (24 on Nectar A/B simulant)
  - Conducted at different beam positions to observe responses to different irradiance distributions
  - Mass loss rates collected with load cell data and scale measurements
  - Water production data was collected using a LN2 chilled cold trap and a Residual Gas Analyzer (RGA)
- Mining rate has been shown to slow down due to deposition on the sacrificial glass used during experiments
  - Excavation rates have been computed for an average (considering the entire test), and a maximum minute-averaged mass loss rate using load cell data
  - These sets were then averaged for tests conducted under the same beam irradiance conditions
- UCS testing performed on Nectar A/B cores to obtain statistical Weibull parameters and thermomechanical properties for use as inputs into the excavation model
- Beam irradiance distributions obtained using a water cooled Gardon gauge sensor

# The Optical Mining Testbed

*Weibull Parameter Testing (Nectar A Results)*

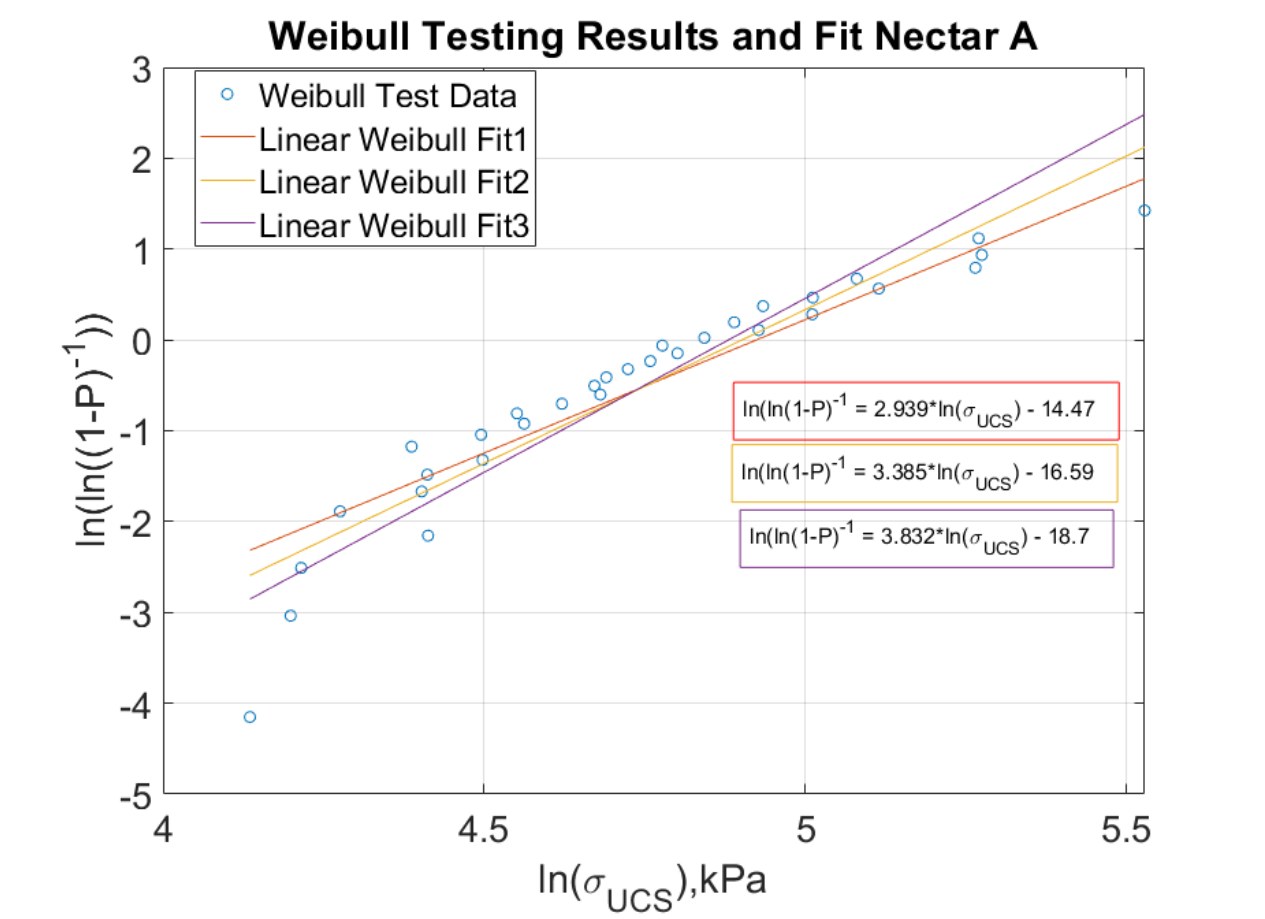


Weibull Function Fit for Nectar A

Weibull Parameter Space:

- m = 2.939, $\sigma_0$ = 137.5 kPa
- m = 3.385, $\sigma_0$ = 134.4 kPa
- m = 3.832, $\sigma_0$ = 131.6 kPa

Where m is the homogeneity factor (the higher the m the more homogenous the material), and $\sigma_0$ is the materials intrinsic strength

# The Optical Mining Testbed

*Weibull Parameter Testing (Nectar B Results)*

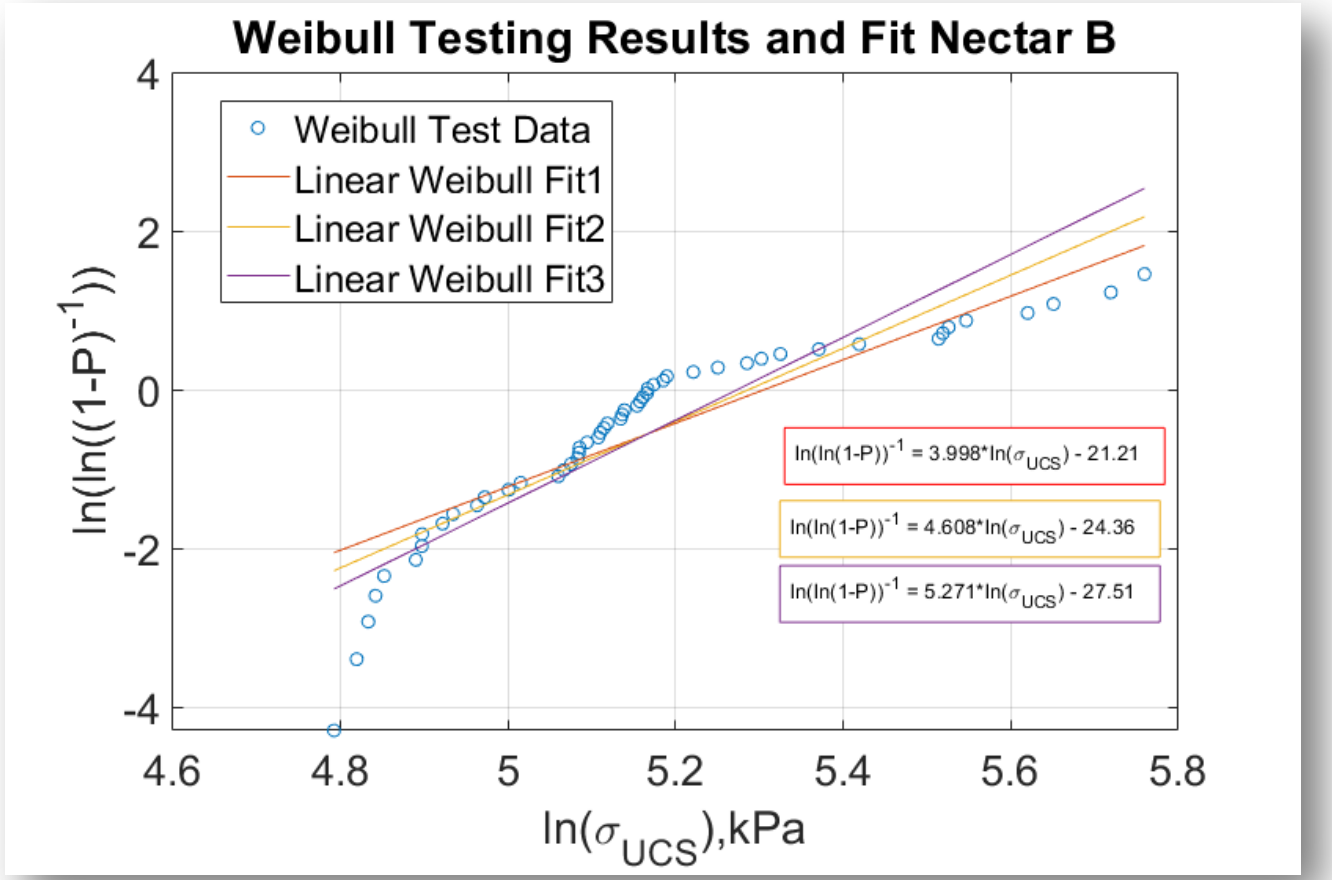


Weibull Function Fit for Nectar B

Weibull Parameter Space:

- m = 3.998, $\sigma_0$ = 201.4 kPa
- m = 4.608, $\sigma_0$ = 197.6 kPa
- m =5.271, $\sigma_0$ = 184.8 kPa

Where m is the homogeneity factor (the higher the m the more homogenous the material), and $\sigma_0$ is the materials intrinsic strength

# The Optical Mining Testbed

*Gardon Gauge Tests*

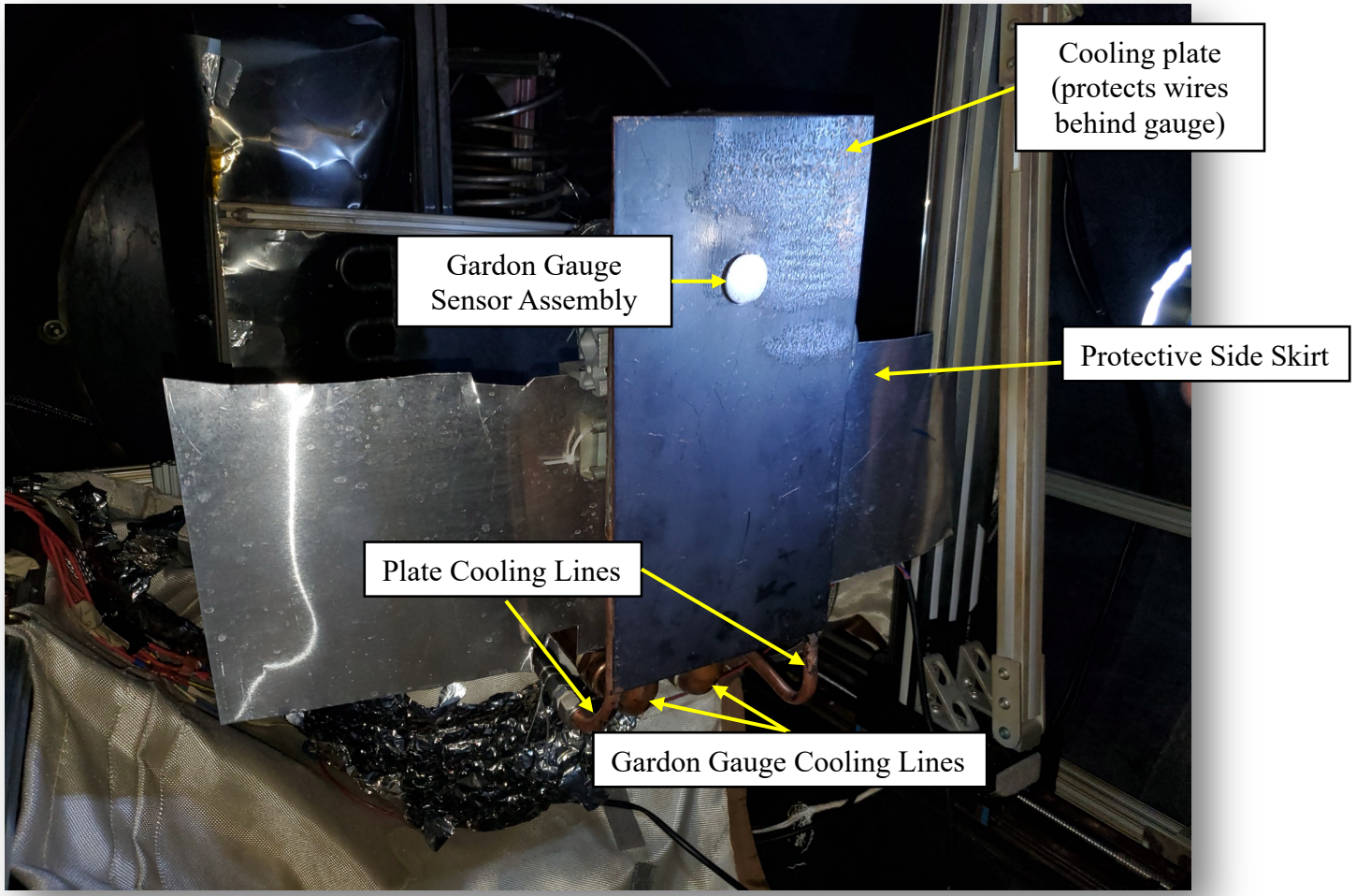


Gardon Gauge Assembly Mounted on a X,Y,Z Motorized Linear Stage

# The Optical Mining Testbed

*Gardon Gauge Tests*

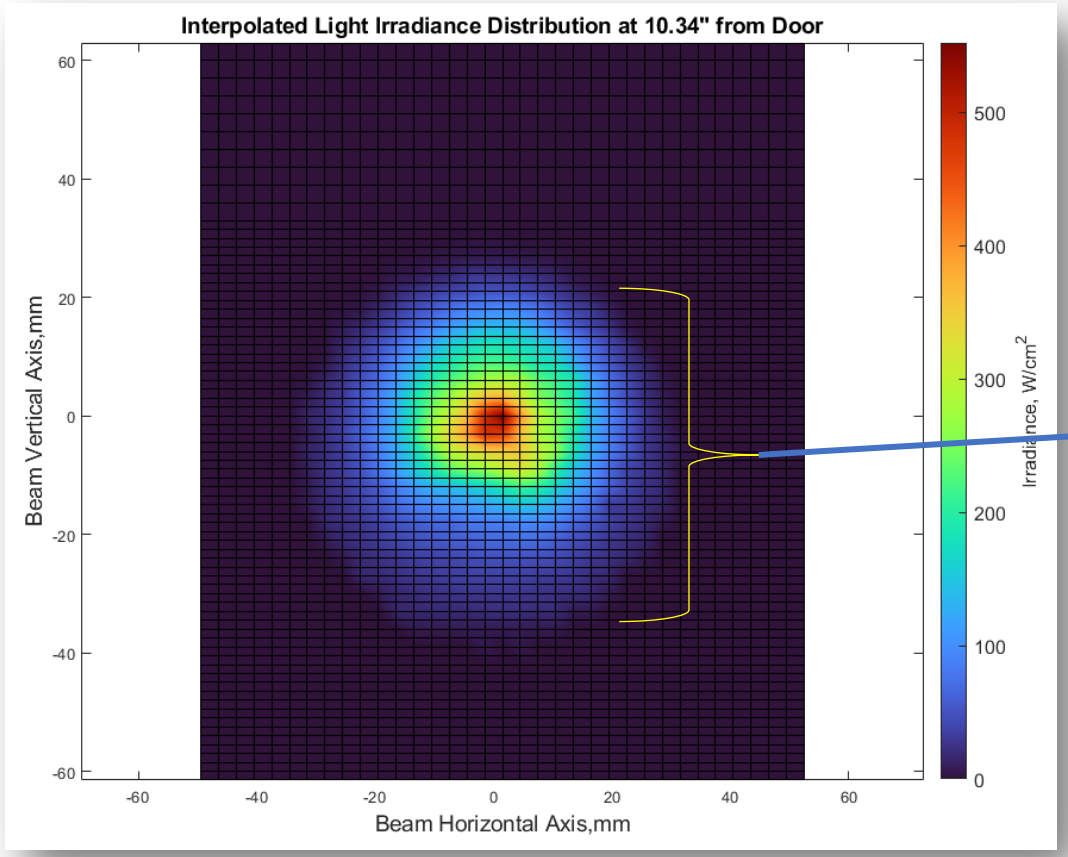


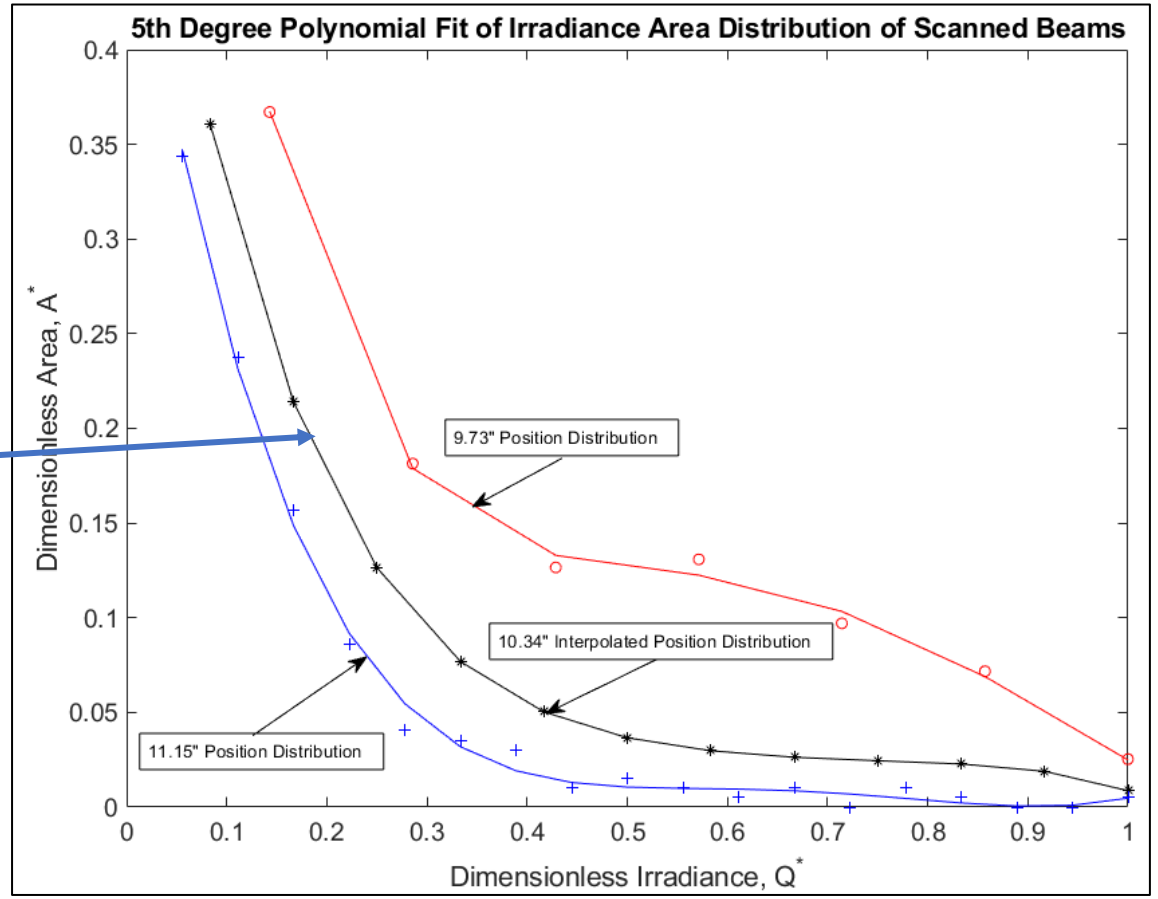


An example Gardon Gauge beam scan results (L) and the distribution of irradiance by area (R)

# The Optical Mining Testbed

*Gardon Gauge Tests*

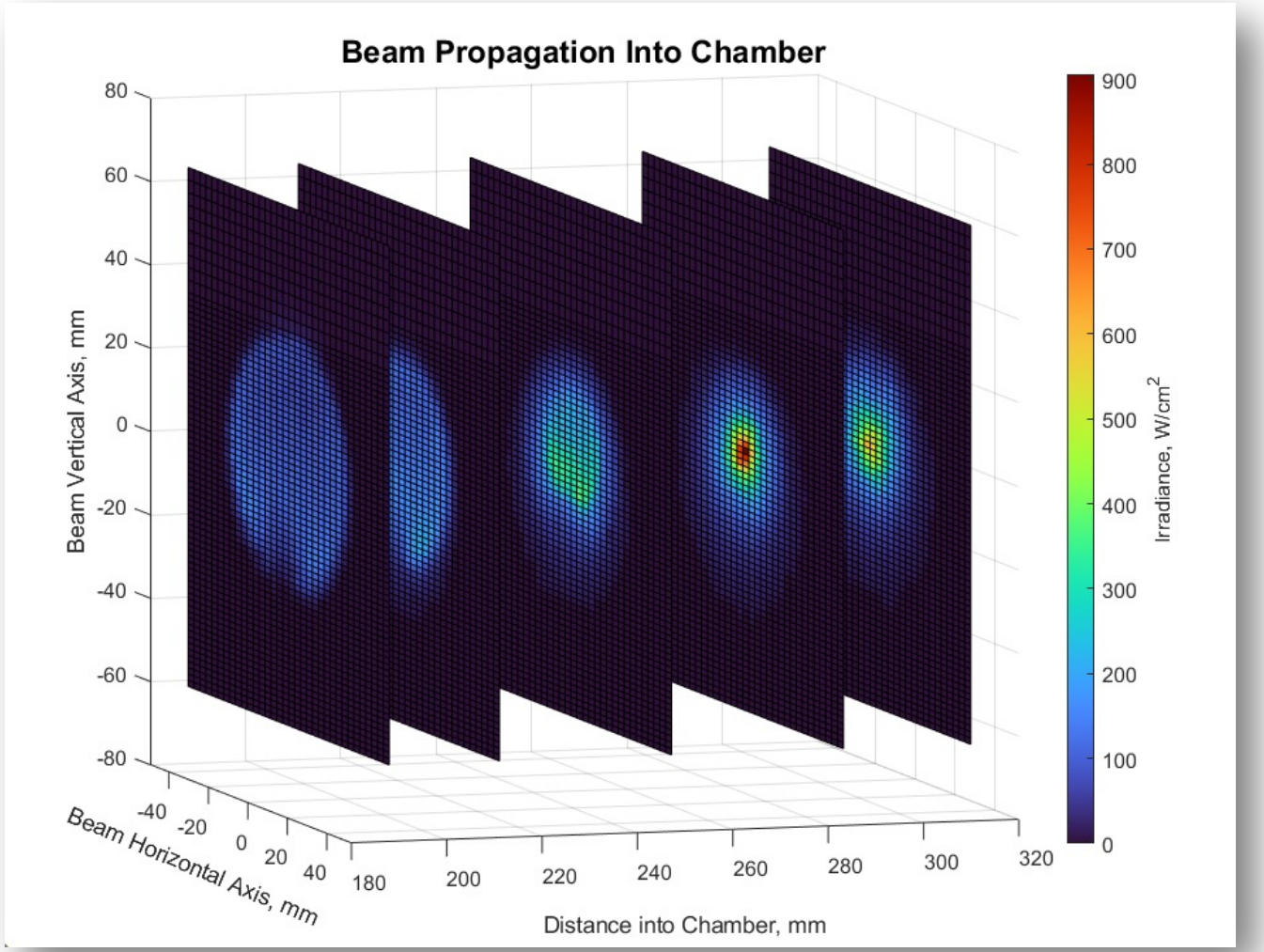


- Creation of a Spall Fragment Volatile production model requires known values of irradiance on spall at each position during its flight path
- Gardon Gauge scans of the beam were used as inputs to interpolate beam irradiances at any position bounded by the scans
  - Allows an estimation of beam irradiance distribution at positions that were not scanned with a Gardon gauge
- Interp3 function in MATLAB used to interpolate irradiance at either a grid of points, or 1 point
  - Assume a linear interpolation is accurate between scanned positions

# The Optical Mining Testbed

*UCS Testing*

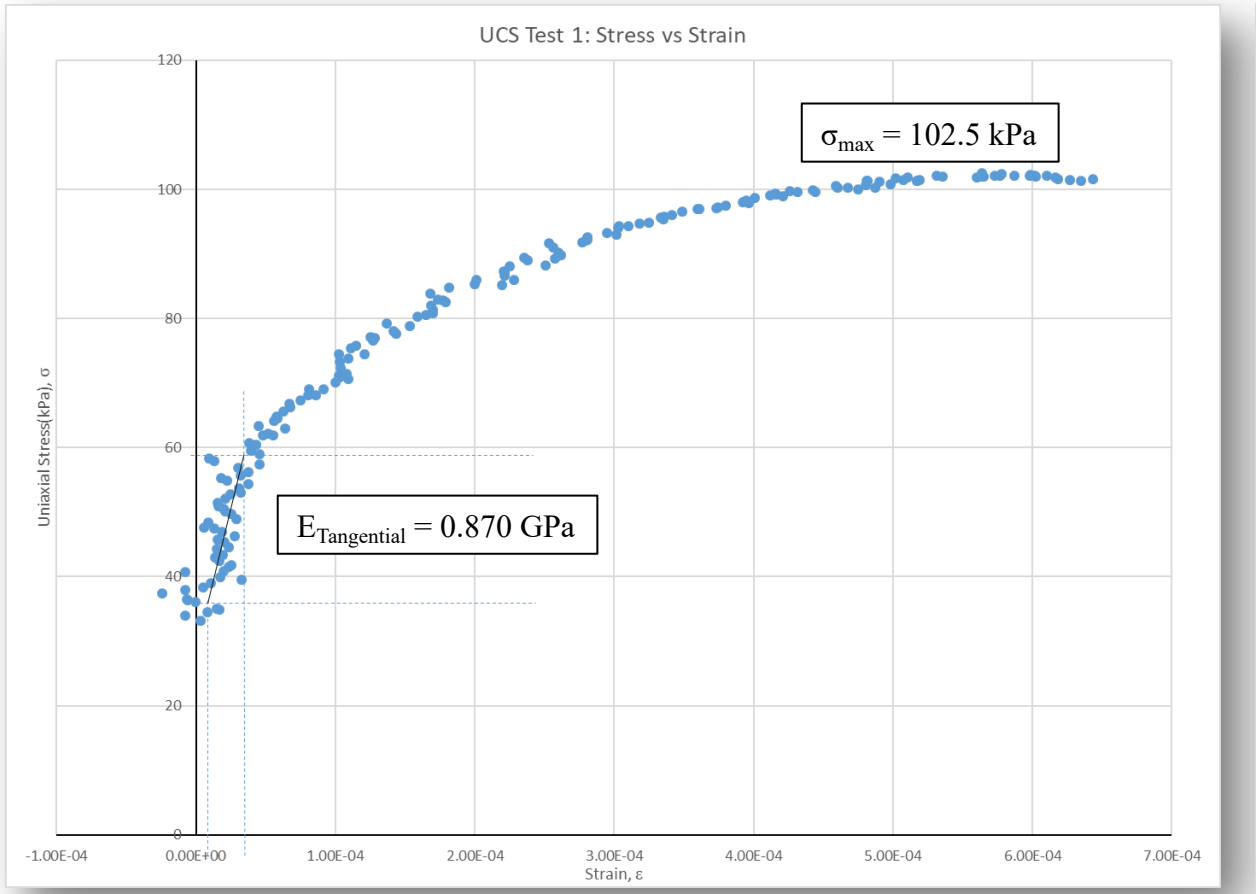


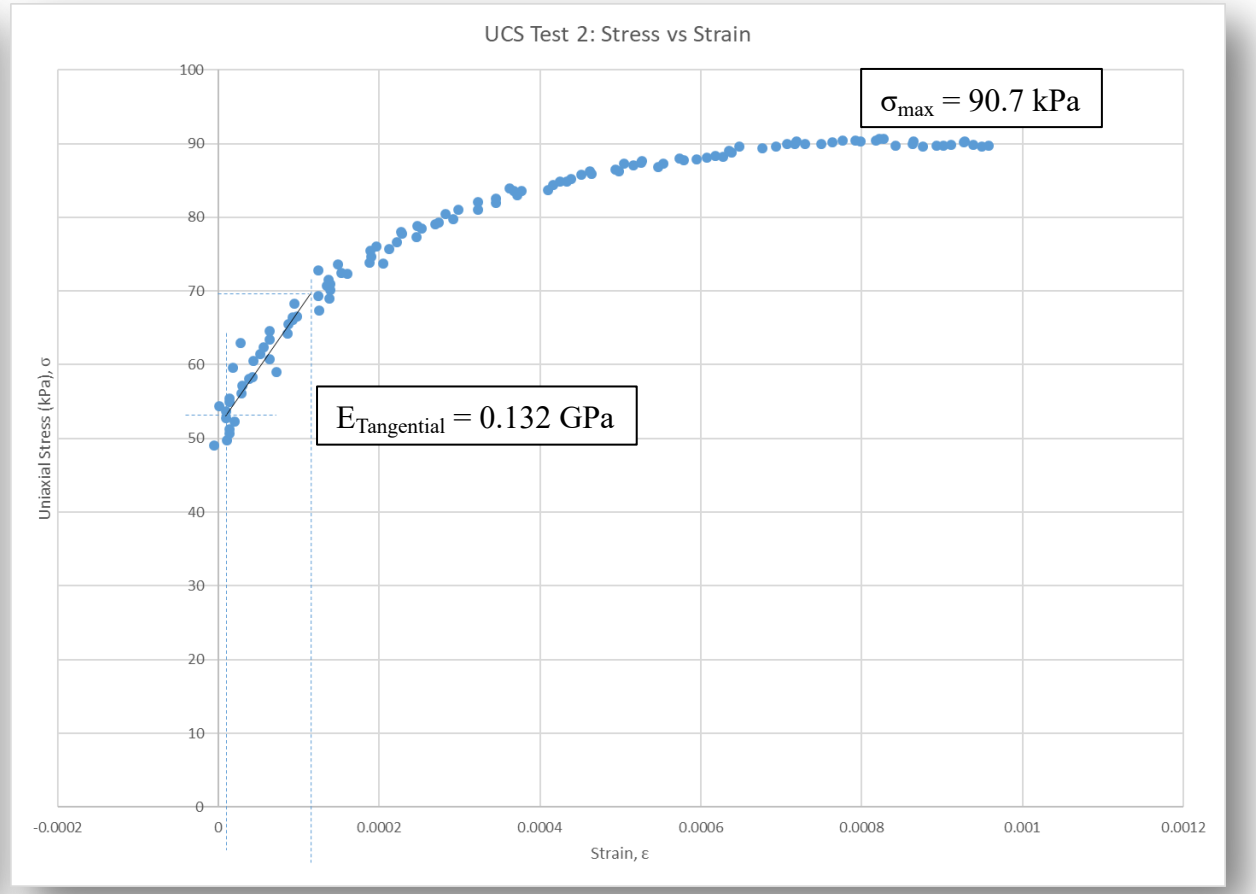


Nectar Core Compressive Strength Testing Results

# The Optical Mining Testbed

*Sample Rotary Stage and Sample Press*

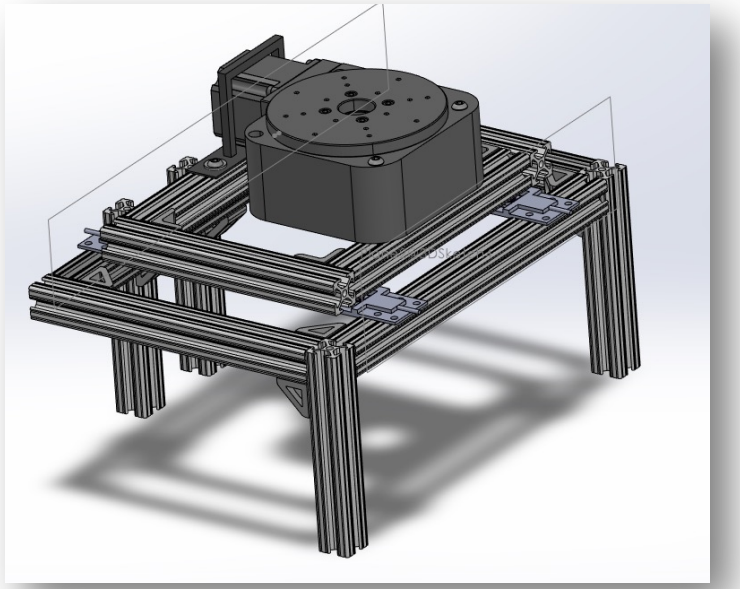

Load Cell Mount CAD

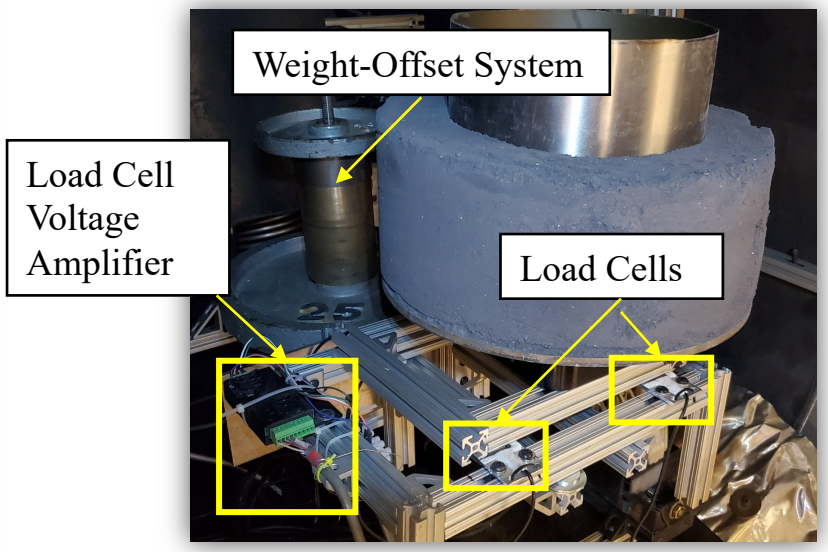


Load Cell Mount System with Weight-Offset


Load Press for Nectar Cake Simulant Production

# The Optical Mining Testbed

*Thermal Expansion Testing*

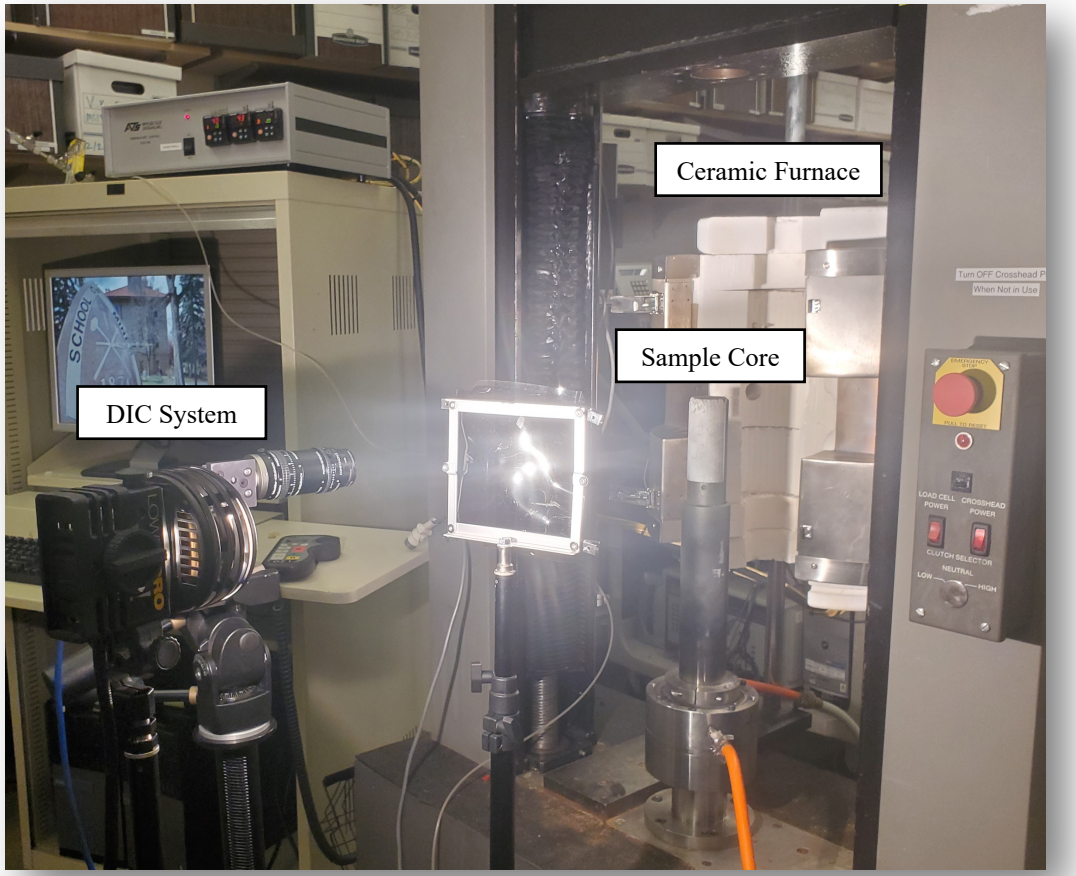


Thermal Expansion Test of a Nectar Core

| Data from Thermal Expansion Tests | |
|---|---|
| **Temp. Range (K)** | **Thermal Expansion Coeff. ($K^{-1}$)** |
| 298 – 423 | $6.36 * 10^{-6}$ |
| 423 – 523 | $9.86*10^{-6}$ |
| 523 – 573 | $1.14*10^{-5}$ |

# The Optical Mining Testbed

*Thermal Conductivity Testing*

Thermal Conductivity Test Using a MP-2 Thermal Conductivity Probe

| Thermal Conductivity Testing Results | |
|---|---|
| **Test Number** | **Thermal Conduction (W/m-K)** |
| 1 | 0.442 |
| 2 | 0.440 |
| 3 | 0.421 |
| Average | 0.434 |

Does no account for decrease of conductivity in vacuum (possible range has been estimated using literature)

# The Optical Mining Testbed

*Load Cell Data*

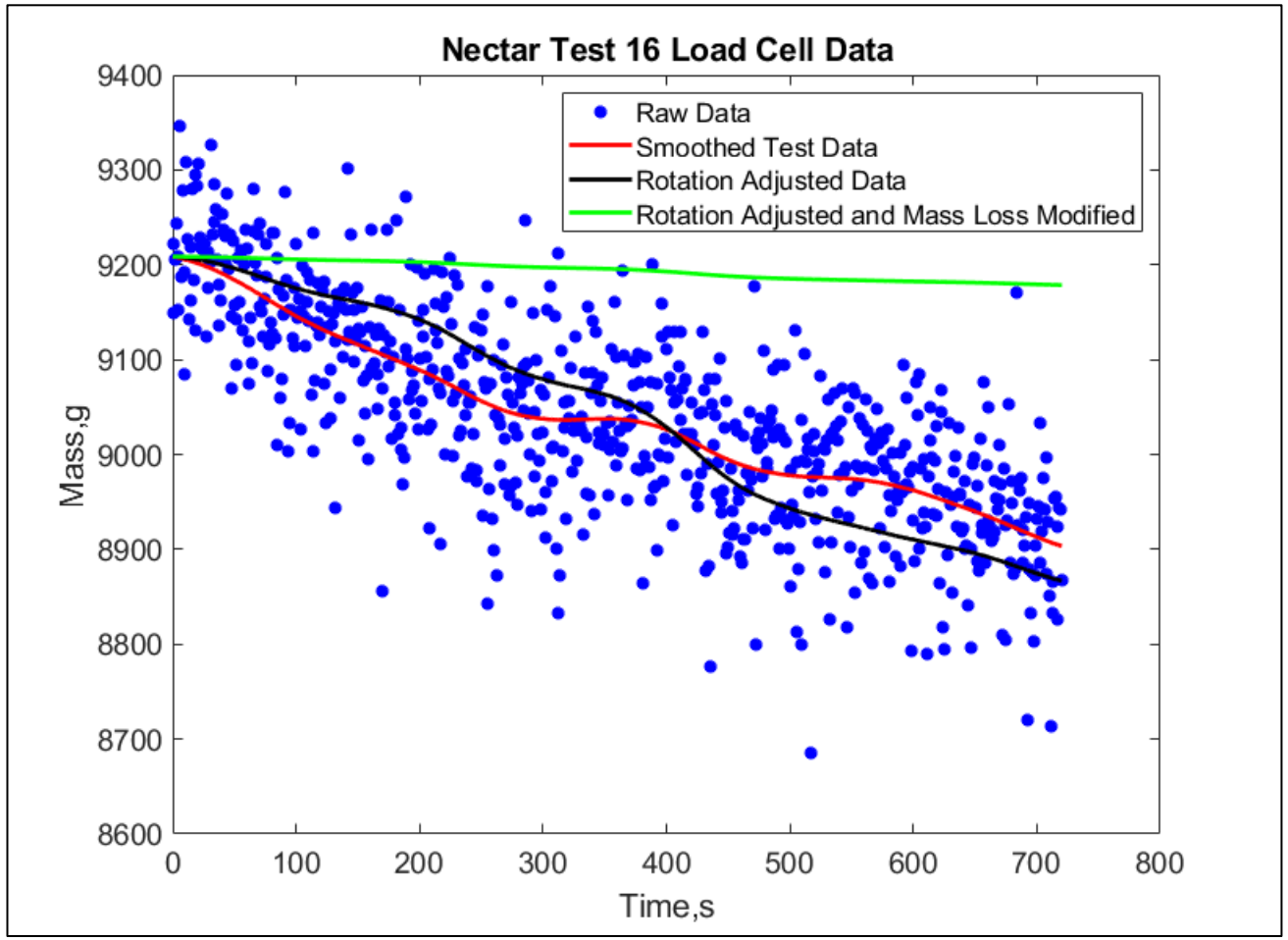


Test 16 Load Cell Data Plot (Nectar B)

- For tests that had a functioning load cell, the Load Cell raw data was smoothed over 3 minute intervals (red line fit), rotational mass variations were subtracted from the data (black line fit), and the data was then adjusted to match the final mass value to the recorded value with a scale (green line fit)
- To obtain mass loss rates, the rotation/mass-loss adjusted values were taken and the gradient determined
- An uncertainty calculation in the mass loss/rotation adjusted load cell measurements was done, however it is not shown here on the plot

# Melt/Alteration Zones

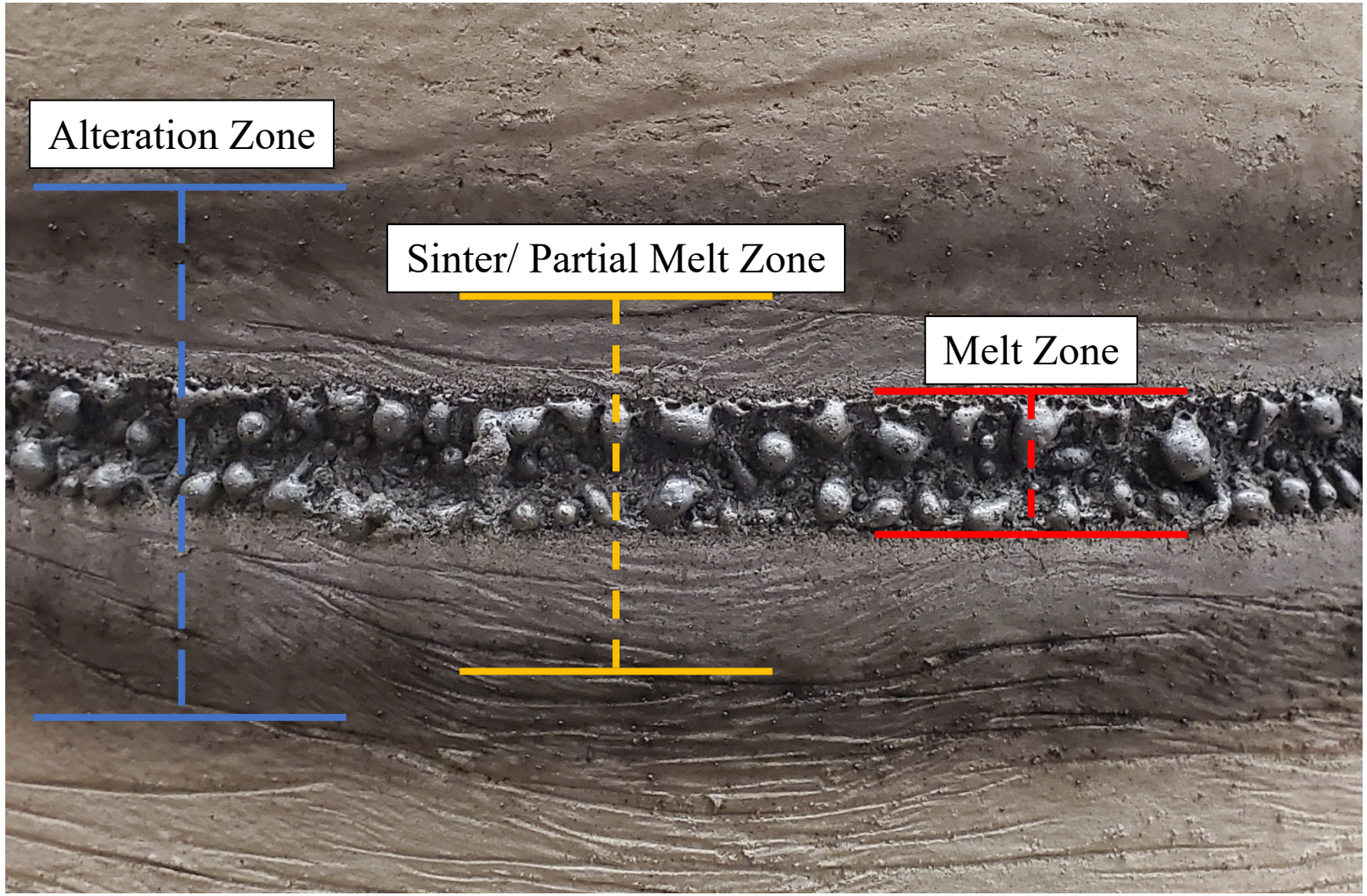


Close-up Post-Test Surface of Nectar B Cake (Test 17)

- 8 equidistant points around the circumference were used to measure the zone sizes
- Average values compiled for each test

| Model Input Parameters | | |
|---|---|---|
| **Parameter** | **Value** | **Notes** |
| Time step (Δt), ms | 0.05 | • Based on stability criteria using Fourier's number<br>• Assumed that model operates on a quasi-static state |
| Spatial Step (Δx), μm | 50 | • Based on median particle size |
| Total Length, cm | 2.2 | • Based on assumption of semi-infinite body<br>• Varied between 10 – 20 x the size of an assumed maximum spall thickness of 1 mm (depending on how long to run the iterative spallation loop) |
| Total Runtime, s | 1-14 | • Depending on how iterative spallation events are modeled |
| Initial Temperature ($T_o$), K | 293 | • Temperature assumed to be (20°C) at start of test |
| Thermal Expansion, $K^{-1}$ | Varies | • Up to Vermiculite expansion onset (280 °C), thermal expansion was based on tests done on Nectar core samples |
| Thermal Conductivity (k), W/m-K | 0.434 | • Based on Nectar core testing<br>• Reduced by 13-56 % to account for vacuum |
| Bulk Density (ρ), $kg/m^3$ | 1181 | • Based on sample manufacture |
| Heat Capacity ($C_p$) , W/kg-K | 1552 | • Based on thermal conductivity testing of Nectar cores |
| Emissivity (ε) | 0.92 | • Based on sandstone properties (w/ grey body assumption) |
| Young's Modulus (E), GPA | 0.201 - 0.870 | • Tangential Youngs modulus based on nectar cores testing<br>• Temperature dependent based on sandstone response to temperature |

| Model Input Parameters | | |
|---|---|---|
| **Parameter** | **Value** | **Notes** |
| Poissons Ratio, ν | 0.21 | • Base on average for sandstone rocks |
| Weibull Variables, (m, $\sigma_o$) | Varied | • Based on Nectar A/B core testing |
| Vermiculite Exfoliation Temperatures, K | 623 - 1000 | • Based on an average temperature from literature review |
| Beam Irradiance, W/cm$^2$ | 25 - 900 | • Based on Gardon gauge test data<br>• Split into dimensionless areas, which change with beam area at different beam positions |
| Beam Area, m$^2$ | Based on Irradiance distribution of Beam | • Imported from Gardon Gauge Test Data |
| Melt Temperature Initiation, $^o$C | 1177 | • Based on onset of melting of significant fraction of material |

# Excavation Model

*Algorithm Overview*

1. Setup of input variables (e.g thermo-mechanical properties, Weibull properties, spallation variables, mesh properties, etc)
2. Initialization of conditions (temperature, stress, conversion factor for dehydroxilation reaction progress, irradiance distribution of beam)
3. Transient temperature calculation for each irradiance bin the beam has been split into at each physical node (checks for temperature dependent properties, reactions, melting)
4. Calculation of thermal stresses looping first through each time step, then irradiance bin, then 1-D volume node into the body
    1. If temperature of a node is within the range of Vermiculite expansion, expansion stresses are calculated based on vermiculite expansion alone (assumption that the expansion stress is much larger than the predetermined thermal expansion stress)
5. Calculates Weibull failure probability function integrating over stressed nodes of each irradiance bin
    a) Summed over all the irradiance bins
6. If Probability is < 0.5, loops through steps 3-5
7. If Probability of failure > 0.5, spallation has occurred
    1. The depth of spallation comprised of the iterated nodes are removed from the total node count and stress at each node point is reset
    2. The node at the depth of spall + dx is set as the new surface node
    3. Record spallation rate, and temperature of surface
8. Repeat steps until end of time is reached

# Excavation Model

*Derivation of Transient 1-D Volumetric Forward Method*

$$\rho C_p \frac{\partial T(r,t)}{\partial t} = -\nabla * q(r,t) + g(r,t)$$

Transient Heat Conduction eqn. w/ energy generation

$$q(r,t) = -k\nabla T(r,t)$$

$$g(r,t) = g_{melt} + g_{reaction}$$

ρ is density, $C_p$ is heat capacity, T is temperature of the finite volume, $\nabla$ is the laplacian operator in Cartesian coordinates, r is the position vector, t is the time, q(r,t) is the heat flux vector (Fourier's Law), and g(r,t) is the volumetric energy generation rate,

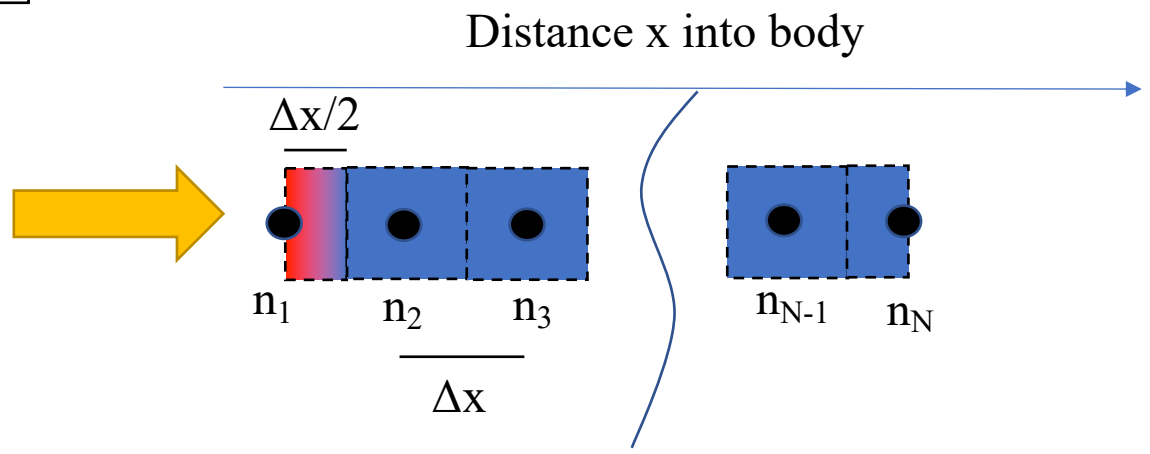


Diagram of heat propagating into a body from a heat flux at the surface

# Excavation Model

*Derivation of Transient 1-D Volumetric Forward Method*

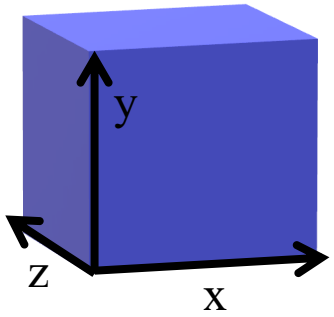

Coordinate System Used

Integrate over a fixed volume

$$\int_0^V \rho C_p \frac{\partial T(r,t)}{\partial t}\, dV = -\int_0^V \nabla * q(r,t)\, dV + \int_0^V g\, dV$$

Assuming that the LHS and source terms can be averaged over the small volume and integrating from 0 $m^3$ to the final Volume gets rid of the coefficients

$$V\rho C_p \frac{\partial \bar{T}(r,t)}{\partial t} = -\int (q(r,t) * n)\, dS + gV$$

$$V\rho C_p \frac{\partial \bar{T}(r,t)}{\partial t} = \int k \frac{\partial \bar{T}}{\partial n}\, dS + gV$$

The volume integral over the divergence of the heat flux vector can be transformed to a surface integral (divergence theorem). S is the surface area of the control Volume. Where: $q(r,t) = -k\nabla T(r,t)$ $\nabla T = \frac{\partial T}{\partial n}$

n is the outward drawn normal vectors at the surface of the control volume

# Excavation Model

*Derivation of Transient 1-D Volumetric Forward Method*

$$V\rho C_p \frac{\partial \bar{T}(r,t)}{\partial t} = \int k \frac{\partial \bar{T}}{\partial x}\, dS + \bar{g}V$$

Assuming the temperature gradients are very small in the y/z dimensions compared to the x dimension

$$\int k \frac{\partial \bar{T}}{\partial x}\, dS$$

Is integrated into 2 parts for the 2 faces of the volumetric cubic element

Part-1

$$k \frac{\partial \bar{T}}{\partial x} \iint dxdy$$

Heat entering 1st surface

Part-2

$$-k \frac{\partial \bar{T}}{\partial x} \iint dxdy$$

Heat leaving 2nd surface

Since the value of dT/dx is constant across the surface, they can be taken out of the integral

# Excavation Model

*Derivation of Transient 1-D Volumetric Forward Method*

Surface-1

$$k\frac{\partial \bar{T}}{\partial x} * A_{bin}$$

Heat entering 1st surface at surface location n-1/2

Surface-2

$$k\frac{\partial \bar{T}}{\partial x} A_{bin}$$

Heat leaving 2nd surface at surface location (n+1/2)

Where $A_{bin}$ is the Area corresponding to the flux bin distribution of the beam

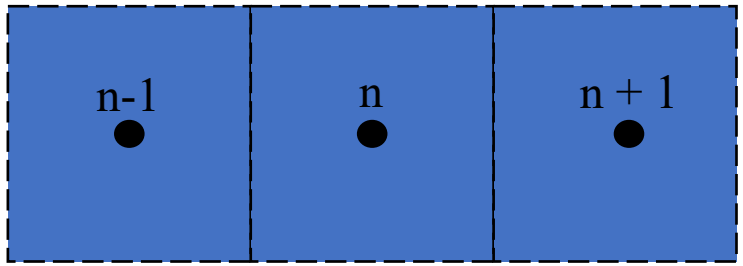


$$V\rho C_p \frac{\partial \bar{T}(r,t)}{\partial t} = kA_{bin}\left(\left(\frac{\partial \bar{T}}{\partial x}\right)_{n+1/2} - \left(\frac{\partial \bar{T}}{\partial x}\right)_{n-1/2}\right) + \bar{g}V$$

$$\frac{\partial \bar{T}(r,t)}{\partial t} = \frac{\alpha}{\Delta x}\left(\left(\frac{\partial \bar{T}}{\partial x}\right)_{n+1/2} - \left(\frac{\partial \bar{T}}{\partial x}\right)_{n-1/2}\right) + \frac{\bar{g}}{\rho C_p} \qquad \alpha = \frac{k}{\rho C_p}$$

Using Central Difference Method for spatial diffusion, and forward difference method for temporal

$$\frac{\partial \bar{T}(r,t)}{\partial t}_n \approx \frac{\bar{T}_n^{j+1} - \bar{T}_n^{j}}{\Delta t}$$

n + 1/2

$$\frac{\partial T}{\partial x_n} \approx \frac{\bar{T}_{n+1}^{j} - \bar{T}_n^{j}}{\Delta x}$$

n - 1/2

$$\frac{\partial T}{\partial x_n} \approx \frac{\bar{T}_n^{j} - \bar{T}_{n-1}^{j}}{\Delta x}$$

# Excavation Model

*Derivation of Transient 1-D Volumetric Forward Method*

Bulk Nodes

$$\frac{\bar{T}_n^{j+1} - \bar{T}_n^j}{\Delta t} = \frac{\alpha}{\Delta x}\left( \left(\frac{\bar{T}_{n+1}^j - \bar{T}_n^j}{\Delta x}\right)_{n+1/2} - \left(\frac{\bar{T}_n^j - \bar{T}_{n-1}^j}{\Delta x}\right)_{n-1/2} \right) + \frac{\bar{g}}{\rho C_p}$$

$$\boxed{\bar{T}_n^{j+1} = \frac{\alpha \Delta t}{\Delta x^2}\left( \left(\bar{T}_{n+1}^j - \bar{T}_n^j\right) + \left(\bar{T}_{n-1}^j - \bar{T}_n^j\right) \right) + \frac{\bar{g}\Delta t}{\rho C_p} + \bar{T}_n^j}$$

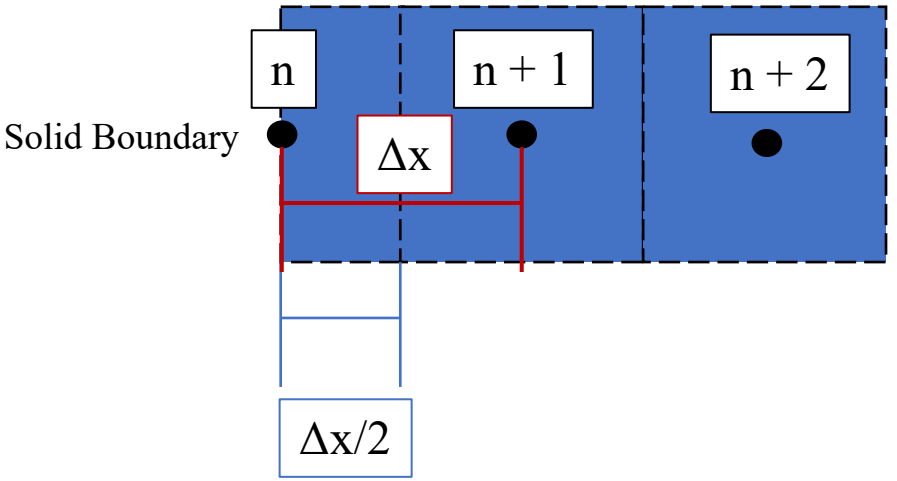


Boundary, n = 1

$$k\frac{dT}{dx} = -(q_{irr} - q_{rad}) \qquad V = \frac{\Delta x}{2} A_{bin}$$

Where $q_{irr}$ = beam irradiance, and $q_{rad}$ is the energy lost due to radiation at the surface

$$V\rho C_p \left.\frac{\partial \bar{T}(x,t)}{\partial t}\right|_{n=1} = A_{bin}\left( (q_{irr} - q_{rad})_n - k\left(\frac{\partial \bar{T}}{\partial x}\right)_{n+1/2} \right) + \bar{g}V$$

# Excavation Model

*Derivation of Transient 1-D Volumetric Forward Method*

Boundary, n = 1

$$V\rho C_p \frac{\partial \bar{T}(r,t)}{\partial t}_{n=1} = A_{bin}\left((q_{irr} - q_{rad})_1 + k(\frac{\partial \bar{T}}{\partial x})_{n+1/2}\right) + \bar{g}V$$

$$\frac{\bar{T}_1^{j+1} - \bar{T}_1^{j}}{\Delta t} = \frac{2}{\Delta x \rho C_p}\left((q_{irr} - q_{rad})_1 + k\frac{\bar{T}_2 - \bar{T}_1}{\Delta x}\right) + \frac{\bar{g}}{\rho C_p}$$

$$\boxed{\bar{T}_1^{j+1} = \frac{2\Delta t}{\Delta x \rho C_p}\left((q_{irr} - q_{rad})_1 + k\frac{\bar{T}_2 - \bar{T}_1}{\Delta x}\right) + \frac{\bar{g}\Delta t}{\rho C_p} + \bar{T}_1^{j}}$$

# Excavation Model

*Derivation of Transient 1-D Volumetric Forward Method*

Boundary, n = N

The boundary is so far away, that the surface can be treated as a semi infinite solid. Hence, it is assumed that its temperature remains constant throughout the modeling timeframe

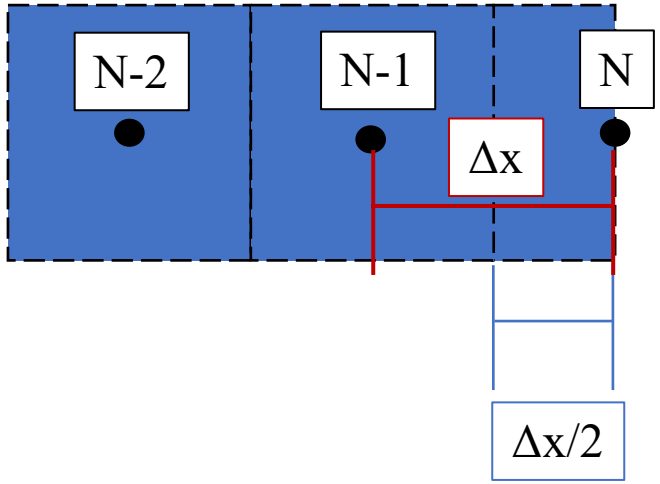


At Boundary: $T(N,t) = T_0$

$$\boxed{T_N^{i+1} = T_0}$$

# Excavation Model

*Stress Calculations*

Without Vermiculite Exfoliation

$$\sigma_{thermal,i} = \frac{E(T) * \alpha_{the}(T) * \Delta T_i}{(1-\nu)}$$

With Vermiculite Exfoliation

$$\sigma_{thermal,i} = \frac{E(T) * \alpha_{the}(T) * \Delta T_i}{(1-\nu)}$$

α increases by several orders of magnitude according to a literature study of Vermiculite expansion

- If Melting Temperature is reached that affects a significant amount of material (currently at 1177 $^{o}$C), it is assumed $\sigma_{thermal,i} = 0$
- At the surface nodes, it is assumed that due to surface undulations there is some expansion that takes place and relieves the thermal stress - $\sigma_{thermal,1} = 0$

$\sigma_{Thermal}$ – Thermal compressive stress, Pa
α– coefficient of thermal expansion
E – Youngs Modulus, Pa
ΔT – Change from initial temperature, K
ν – Poissons ratio

# Excavation Model

*Weibull Probability Function*

- The Weibull Probability distribution function for material will be used to assess specific points at which failure from spalling will occur
- The surface area will be computed from the Volume of stressed material that has Pr > 0.5
- Surface Energy will be computed assuming values of (0.03 – 0.07 J/m$^2$)
- The calculation is performed at 1 node at a time over all the beam irradiance bin before checking if the value of the probability is above 0.5

$$\Pr = 1 - e^{-\int_0^V (\frac{\sigma}{\sigma_0})^m dV)}$$

Using Trapezoidal Rule ⬇

$$\Pr = 1 - e^{-\frac{1}{\sigma_0^m}\Sigma\left(\frac{\sigma_1^m}{2}+\sigma_i^m \ldots.+\frac{\sigma_N^m}{2}\right)dA*dx}$$

m – Homogeneity Factor
A = area of flux
dx = nodal distance
$\sigma_o$ – Stress value at which 37 % of samples fail
Pr – Probability of Failure (0.5 used for spalling)

# Excavation Model

*Equilibrium Chemistry Based Reaction Heat Load*

Boolean (0, or 1)

$$\bar{g}_i = \sum_{k=1}^{Rxn\ number} \frac{E_{rxn.k}\left(X(T)_{k,l} - X(T)_{k,l-1}\right) * n_{reactant}}{\Delta t * V} \delta_k$$

- Average Volumetric heat rate ($\bar{g}_i$)
- Enthalpy of Reaction ($E_{rxn.k}$)
- Current completion fraction of reaction ( $X(T)_{k,l}$)
- Previous completion fraction of reaction ( $X(T)_{k,l-1}$)
- Number of moles of reactant in volume ($n_{reactant}$)
- Boolean for reaction ($\delta_k$ )

The completion fraction of a reaction is based on the linear relationship with the temperature range of the reaction. Where at $T_o$, X = 0 and at $T_f$ , X = 1

# Excavation Model

*Excavation Model Overview – Transient Temperature Calculations*

Bulk Nodes

$$\bar{T}_n^{j+1} = \frac{\alpha \Delta t}{\Delta x^2}\left(\left(\bar{T}_{n+1}^{j} - \bar{T}_n^{j}\right) + \left(\bar{T}_{n-1}^{j} - \bar{T}_n^{j}\right)\right) + \frac{\bar{g}\Delta t}{\rho C_p} + \bar{T}_n^{j}$$

Boundary, n = 1

$$\bar{T}_1^{j+1} = \frac{2\Delta t}{\Delta x \rho C_p}\left((q_{irr} - q_{rad})_1 + k\frac{\bar{T}_2 - \bar{T}_1}{\Delta x}\right) + \frac{\bar{g}\Delta t}{\rho C_p} + \bar{T}_1^{j}$$

Boundary, n = N

$$T_N^{j+1} = T_0$$

$\bar{T}_n^{j}$ - Averaged temperature at node volume for current timestep, K

$\bar{T}_n^{j+1}$ - Averaged temperature at node volume for next timestep, K

$\bar{T}_{n+1\ or\ n-1}^{j+1}$ - Averaged temperature at next or previous node volume for next timestep, K

$\alpha$ – Thermal Diffusivity, $m^2/s$

$\Delta t$ – Timestep, s

$\Delta x$ – Spatial step, m

$\rho$ – Bulk density, $kg/m^3$

$\bar{g}$ - Averaged volumetric heat from reactions, $W/m^3$

$C_p$ – Heat Capacity, J/kg-K

$T_0$ – Initial Temperature, K

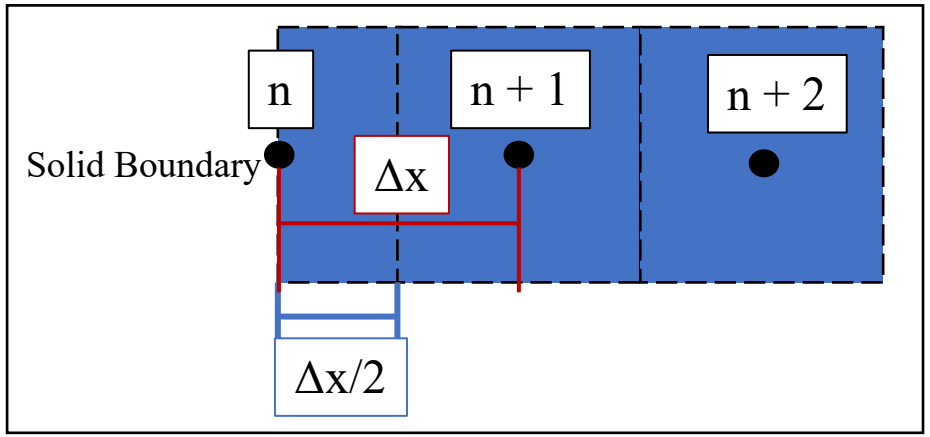


Diagram of Nodal System

# Excavation Model

*Excavation Model Overview – Thermal Stress and Failure Calculation*

Thermal compressive stress (n > 1)

$$\sigma_{Thermal,i} = \frac{\alpha(T)E(T)\Delta T}{1-\nu}$$

$\sigma_{Thermal}$ – Thermal compressive stress, Pa
α– coefficient of thermal expansion
E – Youngs Modulus, Pa
ΔT – Temperature difference between nodes
ν – Poissons ratio

At the surface nodes, it is assumed that due to surface undulations there is some expansion that takes place and relieves the thermal stress

Weibull Failure Probability

$$\Pr = 1 - e^{-\int_0^V (\frac{\sigma}{\sigma_0})^m dV)}$$

*Using Trapezoidal Rule*

$$\Pr = 1 - e^{-\frac{1}{\sigma_0^m}\sum\left(\frac{\sigma_1^m}{2}+\sigma_i^m \ldots.+\frac{\sigma_N^m}{2}\right)dA*dx}$$

m – Homogeneity Factor
A = Area of flux bin, $m^2$
dx = nodal distance, m
$\sigma_o$ – Stress value at which 37 % of samples fail, Pa
Pr – Probability of Failure (0.5 used for spalling)

# Excavation Model

*Effects of Vermiculite Expansion*

- Vermiculite experiences 20 – 30 x expansion in volume due to flash heating [14-15]
  - Steam pressure buildup within the layered structure of the mineral
- <u>Addition into model:</u>
  - If temperature range of nodal volume is within the range of exfoliation, inflate the thermal expansion coefficient to a value determined from expansion ratios of Vermiculite
  - Adjust the inflated value by the volume percentage of Vermiculite present in a nodal volume
  - Stress relief at the surface node due to undulations allowing surface to expand
  - Decrease thermal conductivity and density of expanding node at the surface (based on a relationship between density and thermal conductivity)

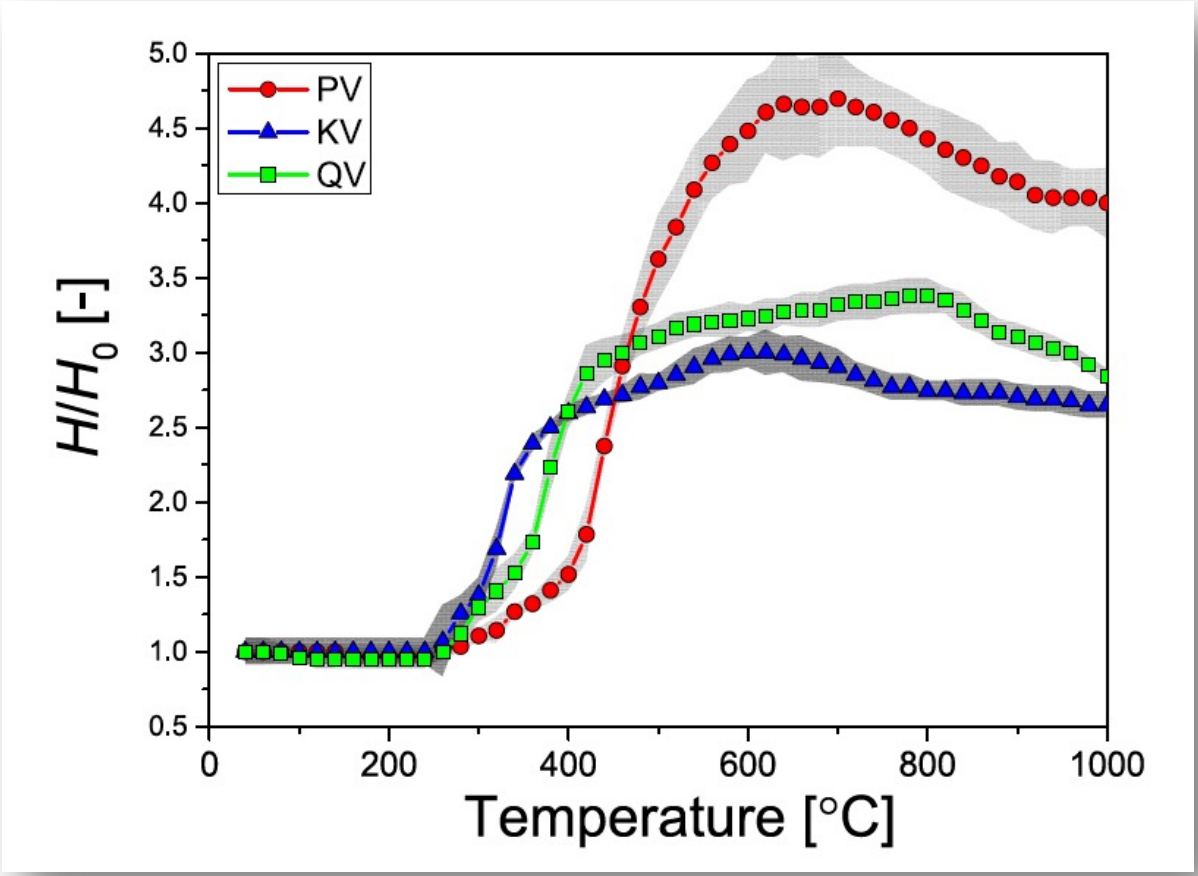


Normalized sample height ($H/H_0$) of Exfoliating Vermiculite Samples of different origins (PV,QV,KV) [15]

# Excavation Model

*Model Assumptions and Simplifications*

- Heating is 1-D dominant (heat transfer into depth of body)
- Homogenous Material Properties
- Stresses go to zero when most of a nodal volume reaches melting/sintering temperature
- Any nodes that have a majority melt do not contribute to spallation mass loss calculations
- Surface undulation allows particles to expand at the surface and relieve stress
  - This has been an observation during experiments
- Thermo-mechanical property change to temperature is very close to that of sandstones
- All stress energy is released once a spallation event has occurred
- Thermal expansion differences between minerals not accounted for, as this would require knowledge of each mineral position (and 2-D or 3-D model)
  - Could possibly incorporate in a future model iteration by assuming a certain distribution of minerals in a nodal volume, and contact area
- Equilibrium assumption for chemical reactions
- Thermal stress is averaged over a node volume (no stress concentrations)